LA-UR- 11-04195

Approved for public release; distribution is unlimited.

Title: Representing Shear Localization under Dynamic Loading Conditions

Author(s): C. A. Bronkhorst
H. M. Mourad
F. L. Addessio
B. L. Hansen
E. K. Cerreta
J. F. Bingert

Intended for: THERMEC 2011
Quebec City, Canada

Los Alamos
NATIONAL LABORATORY
EST. 1943

Representing Shear Localization under Dynamic Loading Conditions

C. A. Bronkhorst[1], H. M. Mourad[1], F. L. Addessio[1], B. L. Hansen[1], E. K. Cerreta[2], J. F. Bingert[2]
[1]Theoretical Division, Fluid Dynamics and Solid Mechanics
[2]Materials Science and Technology Division, Structure/Property Relations
Los Alamos National Laboratory, Los Alamos, NM 87545, USA
Email: cabronk@lanl.gov, hmourad@lanl.gov, addessio@lanl.gov, bhansen@lanl.gov, ecerreta@lanl.gov, bingert@lanl.gov

The localization and adiabatic shear banding process is studied for both annealed tantalum and 316L stainless steel in the annealed, rolled, and pre-shocked conditions. Tantalum does not form adiabatic shear bands and the dynamic response of this material is examined using both continuum and crystal plasticity computational tools to examine the large deformation response of this material and the corresponding microstructural evolution with deformation. It is found that models which are based upon thermally activated physics of dislocation motion represent well the response of this material under the conditions examined. Comparisons between numerical simulations and experimental data (i.e. flow stress, crystallographic texture, metallographic strain measurements) made on the deformed samples compare reasonably well to the experimental results. Results also suggest that complex and statistically varying evolution of stress state is predicted. Adiabatic shear banding does occur in the three different initial state 316L stainless steel materials. These experiments are considered in the context of both traditional high resolution numerical representation and also a sub-grid technique which is implemented within an explicit Lagrangian framework. This sub-grid method is based on the assumed-strain approach of Fish and Belytschko (1988), which allows for localization bands to be embedded within an element, thereby alleviating mesh sensitivity and reducing the required computational effort for representation of this very small scale process zone. Computational results are presented and compared to both the tantalum and 316L stainless steel experimental results (LA-UR-10-07418).

Presentation: Oral

Representing Shear Localization under Dynamic Loading Conditions

C. A. Bronkhorst, H. M. Mourad, F. L. Addessio, B. L. Hansen
Theoretical Division

E. K. Cerreta, J. F. Bingert, A. R. Ross
Materials Science & Technology Division

Los Alamos National Laboratory

THERMEC 2011
Quebec City, Canada
2 August, 2011

Outline

- Motivation and challenge
- Macro-scale experiments
- Continuum isotropic constitutive model
  - Anisotropic MTS
- Thermo-viscoplastic single crystal model
  - Thermally activated slip
- Embedded polycrystal forced shear simulations
- Comparison to experimental results
- Summary & comments

Los Alamos NATIONAL LABORATORY EST. 1943
Operated by Los Alamos National Security, LLC for NNSA
NNSA

Explosively Loaded Sample Demonstrates Ductile Damage and Failure Physics

T. Mason

Explosively Loaded Tantalum Experiment
6 mm thick PETN Beneath Sample – Center Detonated
Soft Sample Recovery

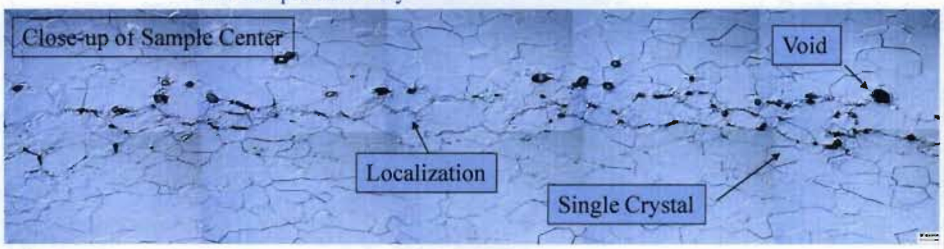

'Void sheets' are forming along grain boundaries in sample

Motivation

- Large-deformation high-rate ductile failure involves
  - Strain localization
  - Void nucleation
  - Void growth
  - Void coalescence
- Predictive modeling of failure requires a good representation of each of these mechanisms
- Modeling strategy
  - Sub-grid computational technique
  - Constitutive / micro-mechanical models

Ta plate impact

Strain Localization in Fragmentation Problems

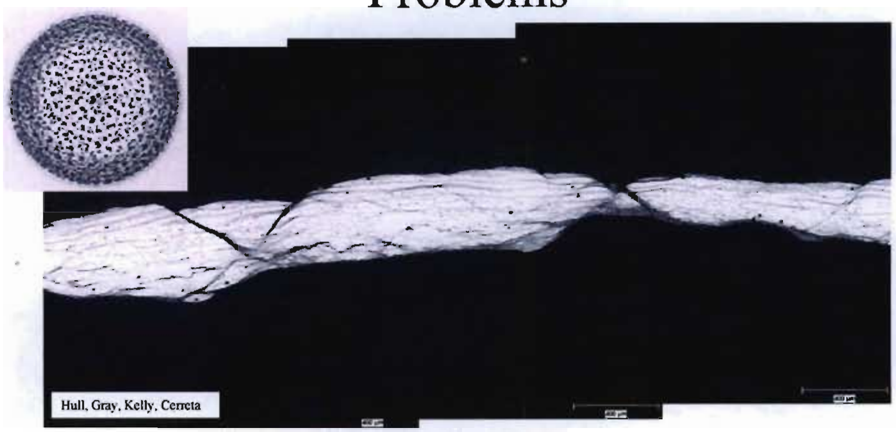

Cross-sectional metallography points to considerable amount of localized plastic work before failure

Challenge of linking microstructure to performance

Ta Plate Impact

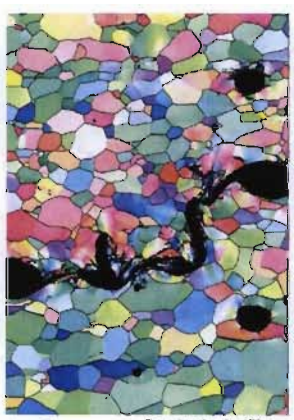

B. Henrie

Cu Plane Strain Compression

Undeformed

$\varepsilon = -1.5$

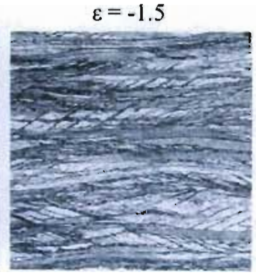

- The ductile failure process generally involves localization, porosity initiation, porosity growth, and coalescence dominated by localized deformation.
- These events occur at the length scale of the single crystal.

Forced shear experiments

- Axisymmetric, Split-Hopkinson
- Top-to-bottom loading, 10-25 m/s
- Tantalum plate, residual texture (Chen & Gray, 1996; Maudlin et al., 1999), grain size 42 μm
- -100 °C and 25 °C

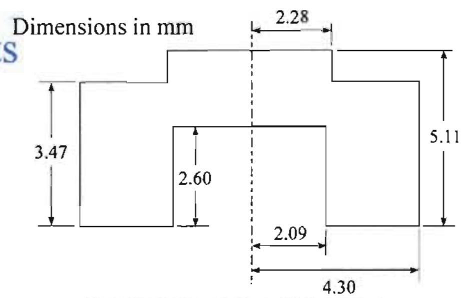

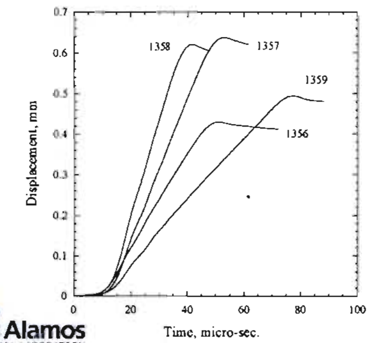

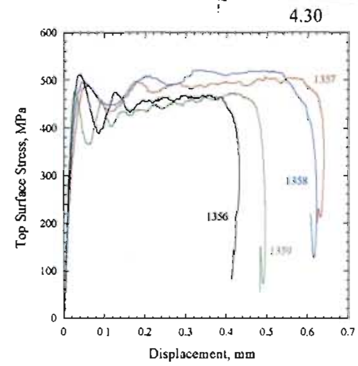

Numerical model with boundary conditions

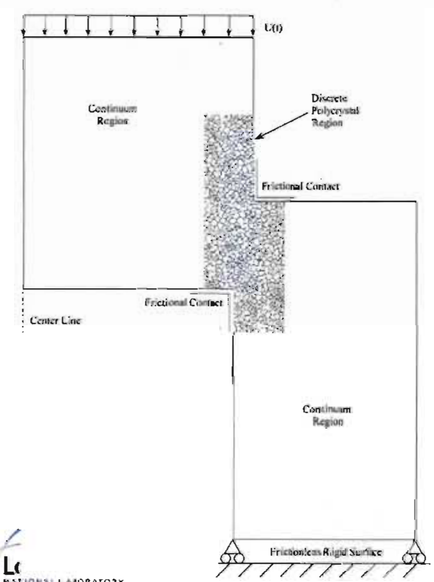

- Axisymmetric, 3 node linear elements for shear zone
- Adiabatic
- Embedded 1091 grain polycrystal region
- 40 μm grain size
- ~ 7 μm element size
- Rate-dependent isotropic continuum regions
- Frictionless contact surfaces at corners
- ABAQUS - implicit used but dynamic displacement rate applied
- 3 crystallographic realizations

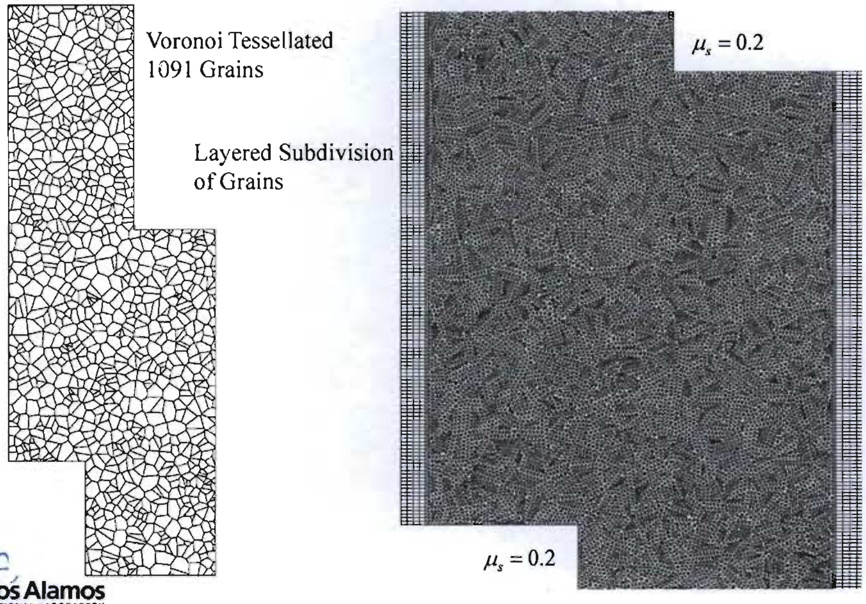

Localization - Ta

- Dynamic response of the SHPB system is not represented
- Piecewise linear velocity profile applied uniformly to the top surface
- Top surface stress response is weighted average of top row of elements

Velocity profile at -100 °C

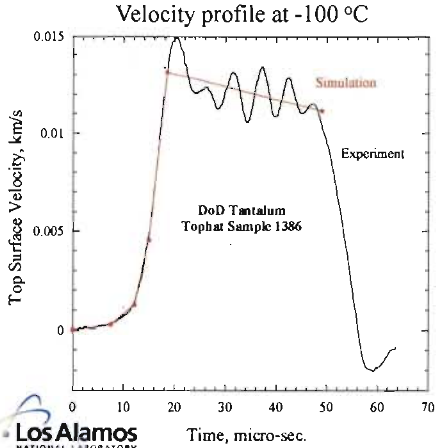

Predicted response at -100 °C

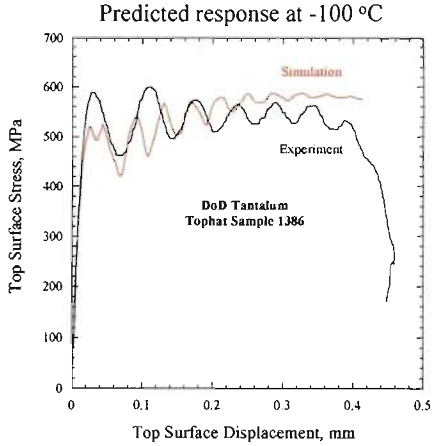

Small strain continuum model for the inner and outer regions

<u>Stress</u>

$$\dot{\boldsymbol{\sigma}} = \underline{\mathbf{C}}\dot{\boldsymbol{\varepsilon}}^{e}$$

<u>Strain</u>

$$\dot{\boldsymbol{\varepsilon}} = \dot{\boldsymbol{\varepsilon}}^{e} + \dot{\boldsymbol{\varepsilon}}^{p}$$

<u>Normality Flow</u>

$$\dot{\boldsymbol{\varepsilon}}^{p} = \frac{3}{2}\dot{\bar{\varepsilon}}^{p}\frac{\boldsymbol{\sigma}'}{\bar{\sigma}}$$

<u>Flow Surface</u>

$$\bar{\sigma} - \sigma_f\left(\dot{\bar{\varepsilon}}^{p}, \theta\right) = 0$$

$$\bar{\sigma} = \sqrt{\tfrac{3}{2}\sigma' \cdot \sigma'}$$

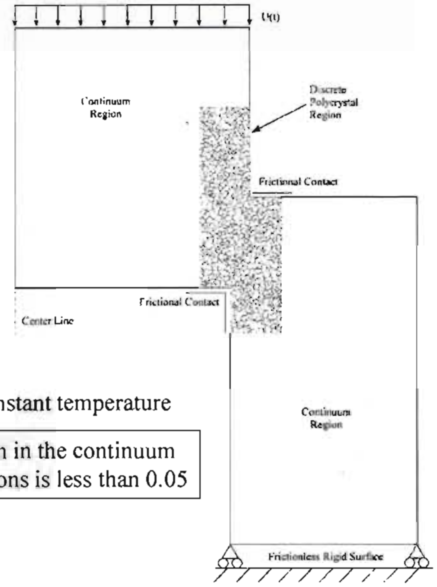

Constant temperature

Strain in the continuum Regions is less than 0.05

MTS model - continuum

Follansbee & Kocks, 1988; Chen & Gray, 1996; Maudlin et al., 1999

$$\sigma_f = \sigma_a + \frac{\mu}{\mu_0}\left(S_i(\dot{\varepsilon},\theta)\hat{\sigma}_i + S_\varepsilon(\dot{\varepsilon},\theta)\hat{\sigma}_\varepsilon\right)$$

$\sigma_a = 40$ MPa $\quad \hat{\sigma}_i = 1203,\ 167$ MPa $\quad \hat{\sigma}_\varepsilon = 0$

$$\mu = \mu_0 - \frac{D_0}{\exp\left(\frac{\theta_0}{\theta}\right) - 1}$$

$\mu_0 = 65.25$ GPa
$D_0 = 0.38$ GPa
$\theta_0 = 40$ °K

$$S_i(\dot{\varepsilon},\theta) = \left(1 - \left[\frac{k\theta}{\mu b^3 g_{0i}}\ln\left(\frac{\dot{\varepsilon}_{0i}}{\dot{\varepsilon}}\right)\right]^{1/q_i}\right)^{1/p_i}$$

$$S_\varepsilon(\dot{\varepsilon},\theta) = \left(1 - \left[\frac{k\theta}{\mu b^3 g_{0\varepsilon}}\ln\left(\frac{\dot{\varepsilon}_{0\varepsilon}}{\dot{\varepsilon}}\right)\right]^{1/q_\varepsilon}\right)^{1/p_\varepsilon}$$

$b = 2.863$ Å
$g_{0i} = 0.1236\ ,\ 5.1463$
$\dot{\varepsilon}_{0i} = \dot{\varepsilon}_{0\varepsilon} = 10^7\ s^{-1}$
$q_i = 3/2$
$p_i = 1/2$
$q_\varepsilon = 1$
$p_\varepsilon = 2/3$

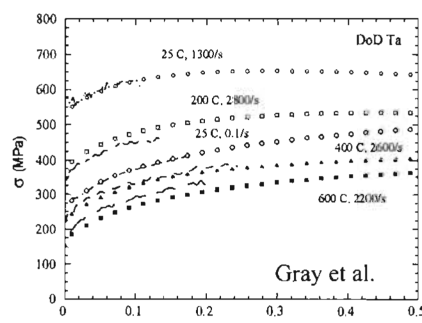

$$\frac{d\hat{\sigma}_\varepsilon}{d\varepsilon} = h_0\left(1 - \frac{\hat{\sigma}_\varepsilon}{\hat{\sigma}_{\varepsilon s}}\right)^{\kappa}$$

$$\frac{\hat{\sigma}_{\varepsilon s}}{\hat{\sigma}_{\varepsilon s_0}} = \left(\frac{\dot{\varepsilon}}{\dot{\varepsilon}_{0_{\varepsilon s}}}\right)^{\frac{kT}{\mu b^3 g_{0_{\varepsilon s}}}}$$

$h_0 = 2.0$ GPa
$\kappa = 3$
$\hat{\sigma}_{\varepsilon s_0} = 350$ MPa
$\dot{\varepsilon}_{0_{\varepsilon s}} = 10^7$
$g_{0_{\varepsilon s}} = 1.6$

Shear zone single crystal model

Asaro & Rice (1977) , Acharya & Beaudoin (2000),
Kothari & Anand (1998), Busso et al. (2000), Kocks (1976)
Kalidindi et al. (1992), Bronkhorst et al. (1992), Anand (1998)

Stress

$$\mathbf{T}^* = \underline{\mathbf{L}}\left[\mathbf{E}^* - \mathbf{A}\left(\theta - \theta_0\right)\right] \qquad \mathbf{T}^* \equiv \mathbf{F}^{*-1}\left(\det \mathbf{F}^*\right)\mathbf{T}\mathbf{F}^{*-T}$$

$$\mathbf{E}^* \equiv \frac{1}{2}\left(\mathbf{F}^{*T}\mathbf{F}^* - \mathbf{1}\right) \qquad \mathbf{F}^* = \mathbf{F}\mathbf{F}^{p^{-1}}$$

Texture

$$\mathbf{m}^\alpha = \mathbf{F}^*\mathbf{m}_0^\alpha$$

$$\mathbf{n}^\alpha = \mathbf{F}^{*-T}\mathbf{n}_0^\alpha$$

Hardening

$$\dot{s}^\alpha = \sum_\beta h^{\alpha\beta}\left|\dot{\gamma}^\beta\right| \qquad h^{\alpha\beta} = \left[r + (1-r)\delta^{\alpha\beta}\right]h^\beta$$

$$h^\beta = h_o\left(\frac{s_s^\beta - s^\beta}{s_s^\beta - s_0^\beta}\right)$$

$$s_s^\beta = \hat{s}_s^\beta(\dot{\gamma},\theta) = s_{s_0}\left(\frac{\dot{\gamma}^\beta}{\dot{\gamma}_0}\right)^{\frac{k\theta}{A}}$$

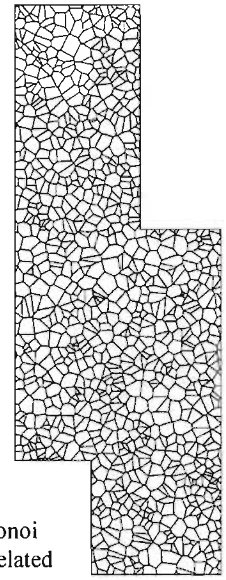

Voronoi tesselated

1091 grains

Shear zone single crystal model

Asaro & Rice (1977) , Acharya & Beaudoin (2000),
Kothari & Anand (1998), Busso et al. (2000), Kocks (1976)
Kalidindi et al. (1992), Bronkhorst et al. (1992), Anand (1998)

Flow Rule

$$\mathbf{L}^p = \dot{\mathbf{F}}^p\mathbf{F}^{p^{-1}} = \sum_\alpha \dot{\gamma}^p\mathbf{S}_0^\alpha \qquad \mathbf{S}_0^\alpha \equiv \mathbf{m}_0^\alpha \otimes \mathbf{n}_0^\alpha$$

$$\dot{\gamma}^\alpha = \dot{\gamma}_0 \exp\left[-\frac{F_0}{k\theta}\left\langle 1 - \left\langle \frac{\left|\tau^\alpha\right| - s^\alpha \frac{\mu}{\mu_0}}{s_l^\alpha \frac{\mu}{\mu_0}} \right\rangle^p \right\rangle^q\right] \operatorname{sgn}\left(\tau^\alpha\right)$$

$$\tau^\alpha \equiv \left(\mathbf{C}^*\mathbf{T}^*\right)\cdot\mathbf{S}_0^\alpha$$

$$\mathbf{C}^* = \mathbf{F}^{*T}\mathbf{F}^*$$

$$\frac{\mu}{\mu_0} \cong \frac{C_{12}}{C_{12_0}} = 1 + \frac{m_{12}}{C_{12_0}}\theta$$

Simmons & Wang, 1971

Adiabatic Heating

$$\dot{\theta} = \frac{\eta}{\rho c_p}\sum_\alpha \tau^\alpha\dot{\gamma}^\alpha$$

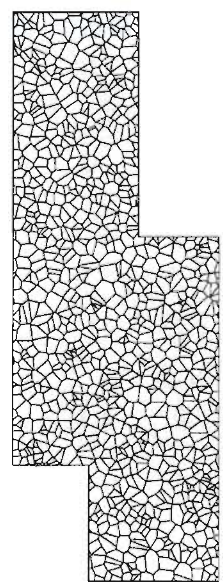

900 μm between corners

Single crystal model - Ta

Single Crystal Model

Initial Texture

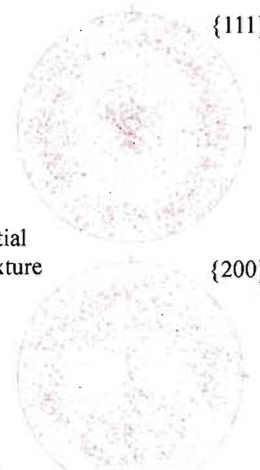

$\rho = 16640$ kg/m^3
$c_p = 150$ J/kg-K
$\alpha = 6.5$ μm/m-K
$\eta = 0.0, 0.95$
$m_{11} = -24.5$ MPa/K
$C_{11_0} = 268.5$ GPa
$m_{12} = -11.8$ MPa/K
$C_{12_0} = 159.9$ GPa
$m_{44} = -14.9$ MPa/K
$C_{44_0} = 87.1$ GPa
$r = 1.4$

$\dot{\gamma}_0 = 10^7$ sec^{-1}
$s_0 = 50$ MPa
$s_l = 550$ MPa
$F_0 = 2.1\times10^{-19}$ J
$p = 0.34$
$q = 1.66$
$s_{s_0} = 125$ MPa
$h_{s_0} = 300$ MPa
$A = 10^{-18}$ J

Material Parameter Evaluation
512 Elements/Grains

Ta - 24 BCC systems
{110}<111>, {112}<111>

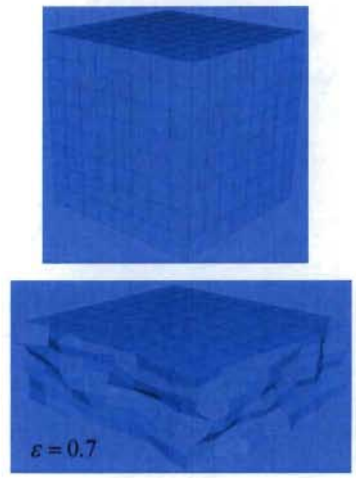

Single crystal model - Ta

Single Crystal Model

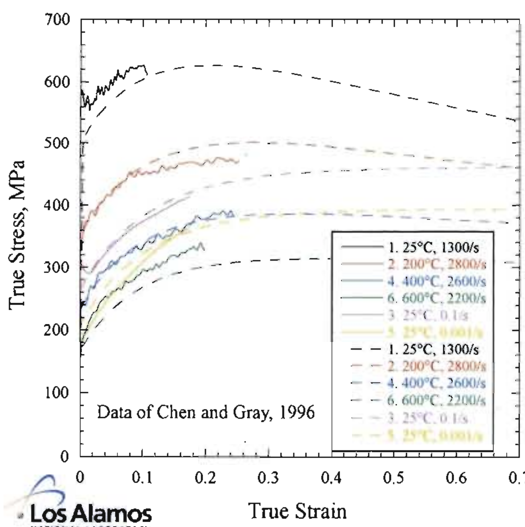

Material Parameter Evaluation

Ta - 24 BCC systems
{110}<111>, {112}<111>

$\rho = 16640$ kg/m^3	$r = 1.4$
$c_p = 150$ J/kg-K	$\dot{\gamma}_0 = 10^7$ sec^{-1}
$\alpha = 6.5$ μm/m-K	$s_0 = 50$ MPa
$\eta = 0.0, 0.95$	$s_l = 550$ MPa
$m_{11} = -24.5$ MPa/K	$F_0 = 2.1\times10^{-19}$ J
$C_{11_0} = 268.5$ GPa	$p = 0.34$
$m_{12} = -11.8$ MPa/K	$q = 1.66$
$C_{12_0} = 159.9$ GPa	$s_{s_0} = 125$ MPa
$m_{44} = -14.9$ MPa/K	$h_{s_0} = 300$ MPa
$C_{44_0} = 87.1$ GPa	$A = 10^{-18}$ J

Experimental load-displacement response is over-predicted

- Although the loading rate difference is described, overall the model over-predicts the magnitude of load required to deform the sample.
- This is believed to be caused primarily by 2D representation.
- The single crystal model could also be inadequate to well represent this level of detail.

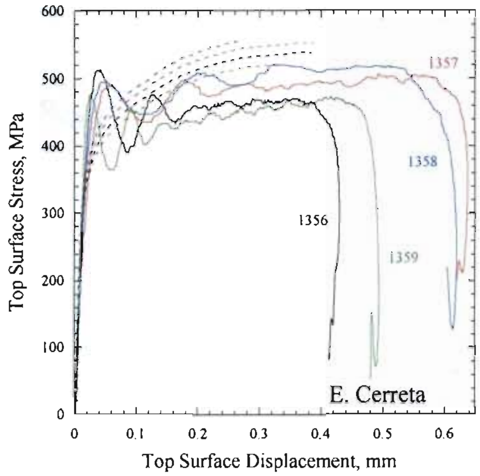

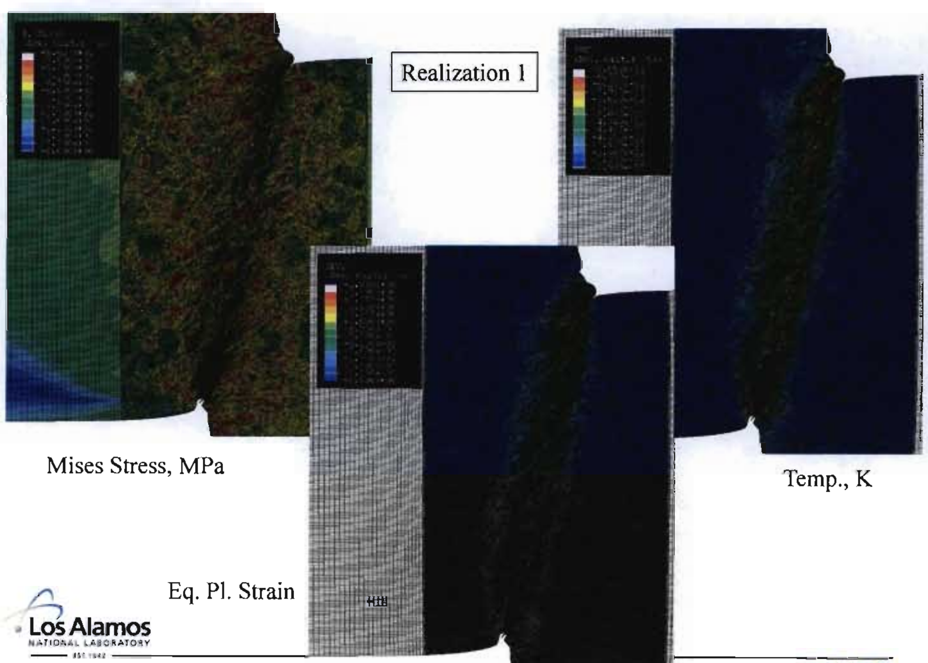

Los Alamos NATIONAL LABORATORY
Operated by Los Alamos National Security, LLC for NNSA
NNSA

Localization - Ta

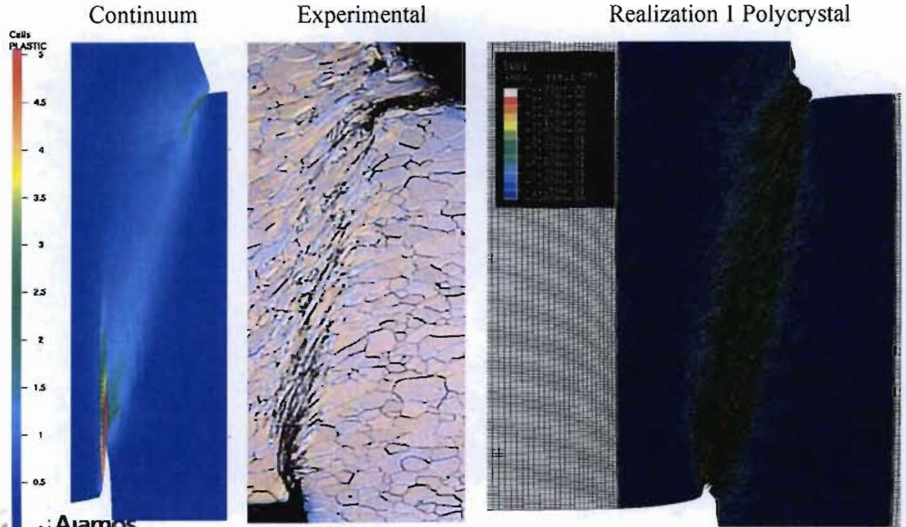

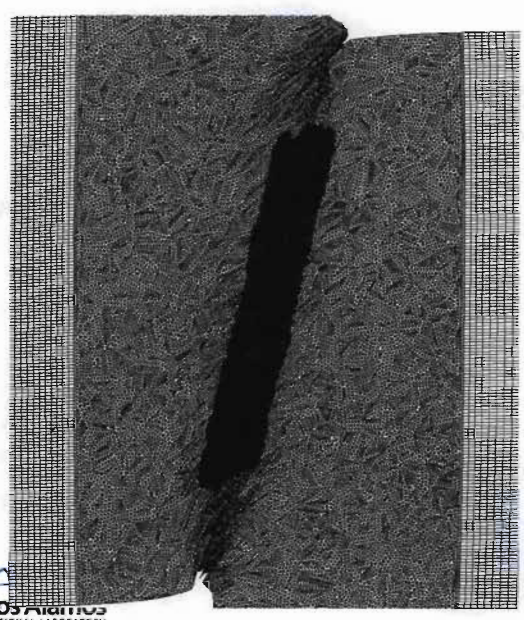

Portion of the shear zone isolated for closer examination.

Statistics of material state
- von Mises stress
- Plastic strain
- Temperature
- Plastic strain rate

Comparison to measurement
- Crystallographic texture
- Strain profile by metallography

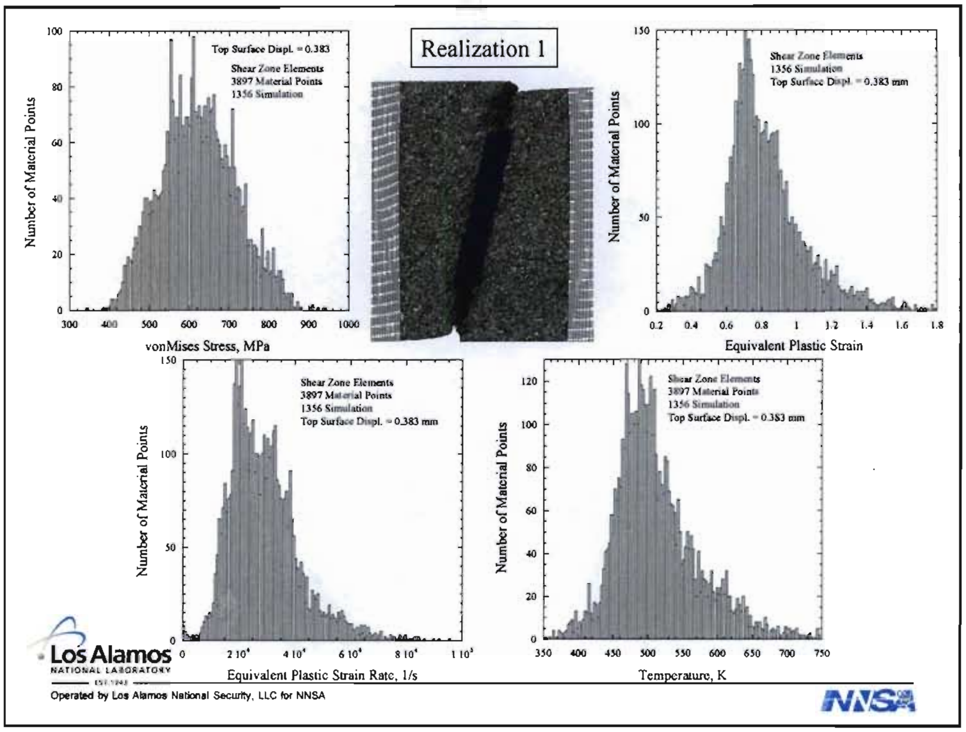
Realization 1
Top Surface Displ. = 0.383
Shear Zone Elements
3897 Material Points
1356 Simulation
Number of Material Points
vonMises Stress, MPa
Shear Zone Elements
1356 Simulation
Top Surface Displ. = 0.383 mm
Equivalent Plastic Strain
Equivalent Plastic Strain Rate, 1/s
Temperature, K
Los Alamos
NATIONAL LABORATORY
Operated by Los Alamos National Security, LLC for NNSA
NNSA

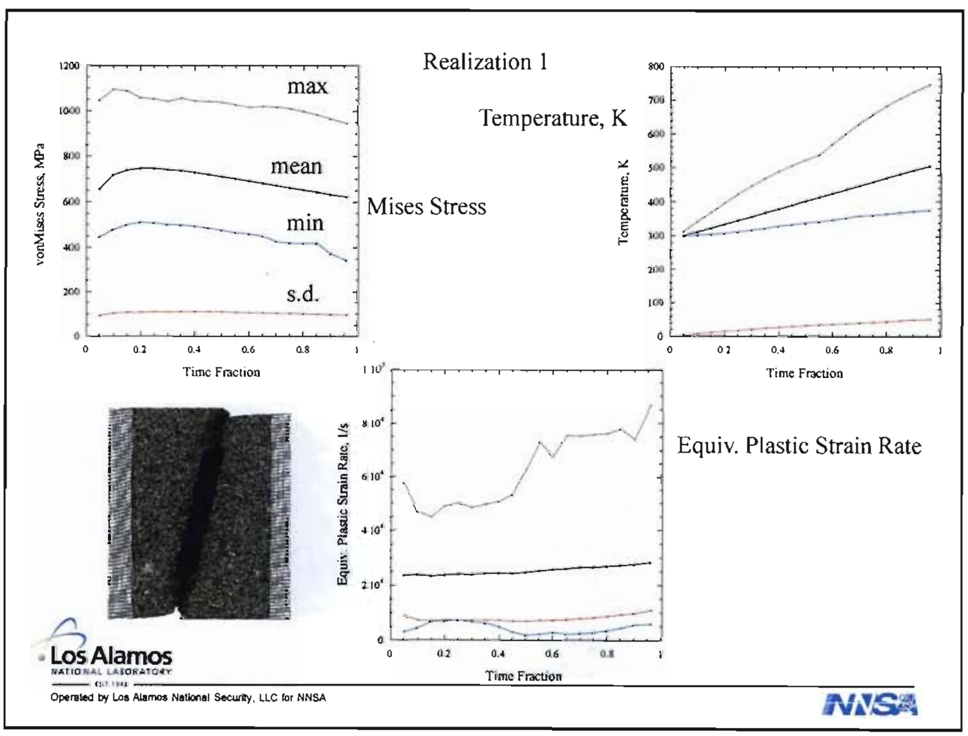
Realization 1
max
mean
min
s.d.
vonMises Stress, MPa
Time Fraction
Mises Stress
Temperature, K
Temperature, K
Time Fraction
Equiv. Plastic Strain Rate, 1/s
Time Fraction
Equiv. Plastic Strain Rate
Los Alamos
NATIONAL LABORATORY
Operated by Los Alamos National Security, LLC for NNSA
NNSA

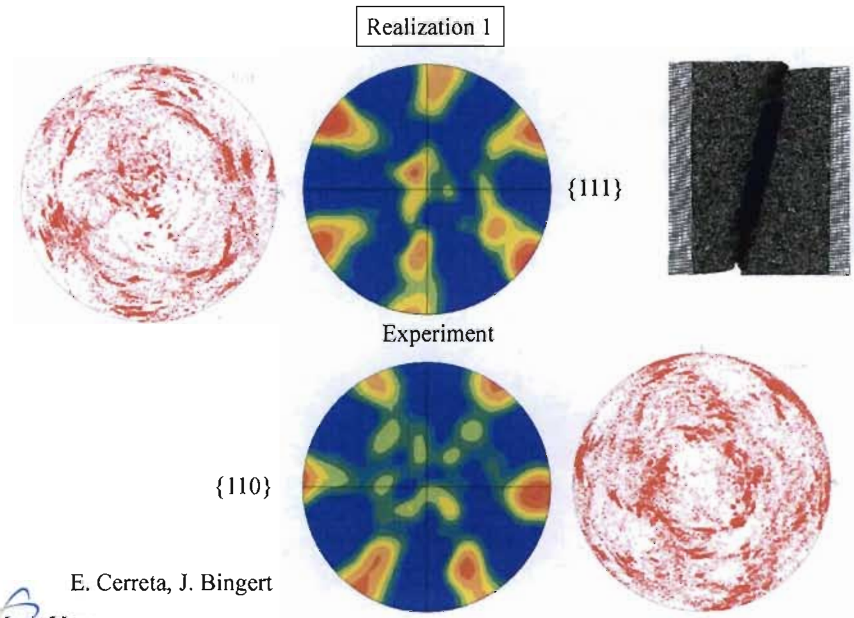

E. Cerreta, J. Bingert

Measurement of Granular Aspect Ratio

Ross

Grain morphology (aspect ratio) was measured along lines parallel to shear zone

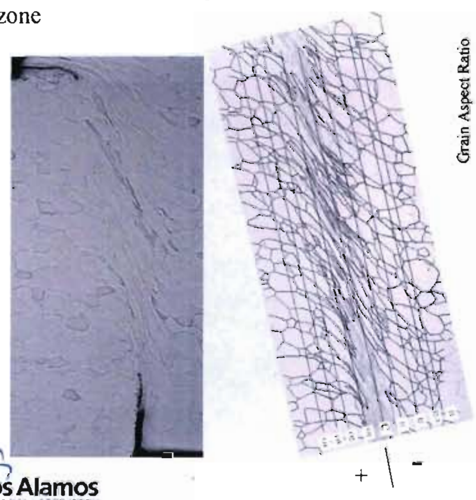

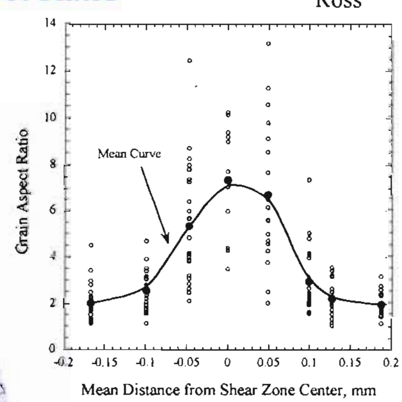

$\varepsilon_l = \frac{2}{3}\ln\left(\frac{AR}{\overline{AR_0}}\right)$ Lower bound

$\varepsilon_u = \frac{2}{3}\ln\left(AR\cdot\overline{AR_0}\right)$ Upper bound

$\overline{AR_0} = 1.9$

3 Differing Crystallographic Realizations

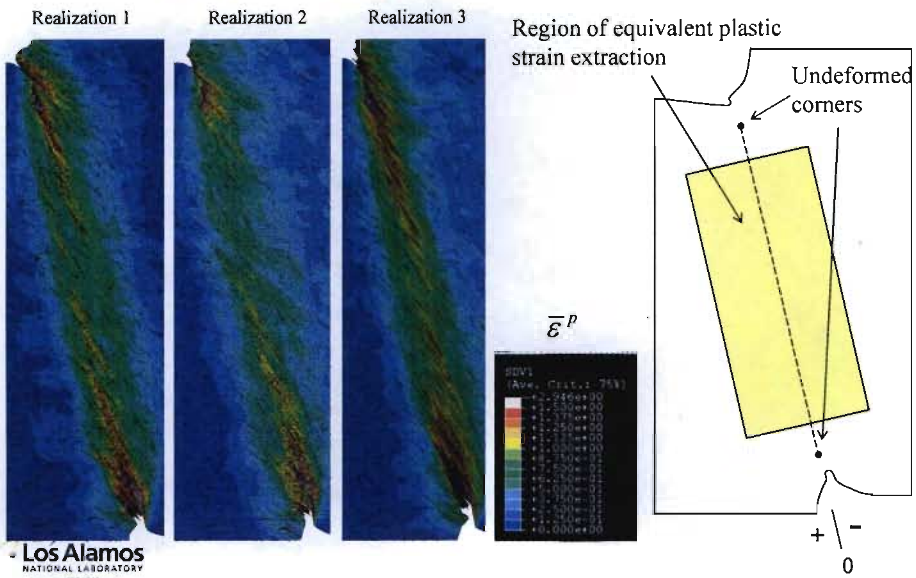

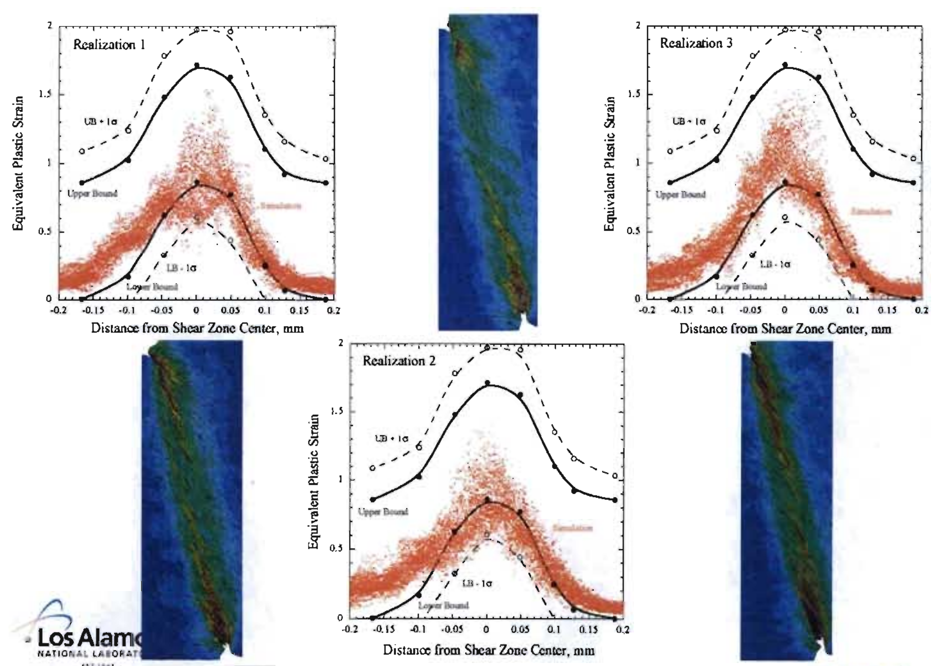

Shear zone region interrogation by nano-indentation

- Hysitron triboindenter – Berkovich pyramidal tip
- 10 measurement zone width – 4 micron step
- Penetration depth – 200 nm
- Loading/unloading rate – 10 nm/s
- Hold time – 10 s

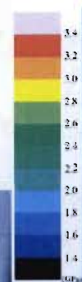

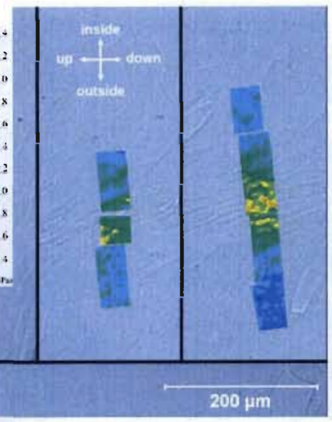

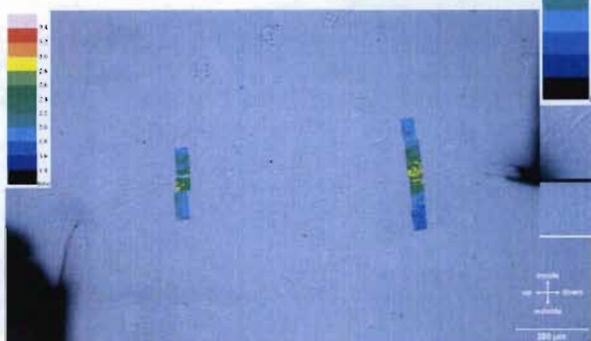

A. Ross
G. Swadener

Shear zone interrogation by nano-indentation

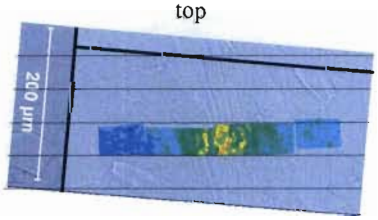

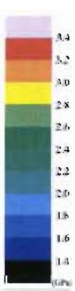

Hardness values are averaged over the 10 measurements at a common distance from the shear zone center = zero position

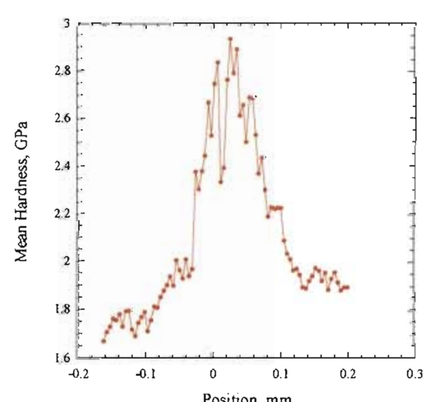

A. Ross, G. Swadener

Top Hat Problem: Experiments vs. Computations

- Experiments
  - Split-Hopkinson pressure bar
  - Top-to-bottom loading (10-25 m/s)
- Computations
  - 46,000 triangular elements in EPIC
  - 2,000 elements in shear section
  - Axisymmetric, adiabatic conditions
  - Frictional self-contact at both corners
  - Piece-wise linear (in time) downward velocity profile applied to top surface
  - Rigid frictionless base
- Compare response (average stress vs. deflection at top surface)

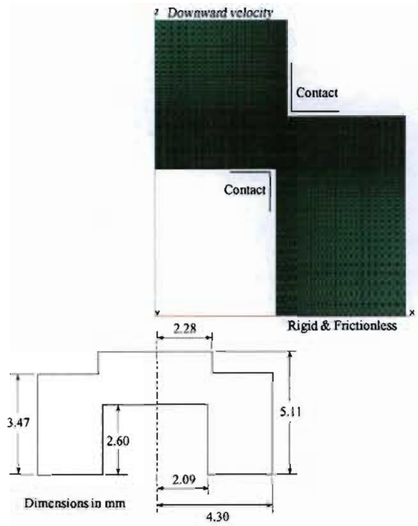

Top Hat Problem: Tantalum

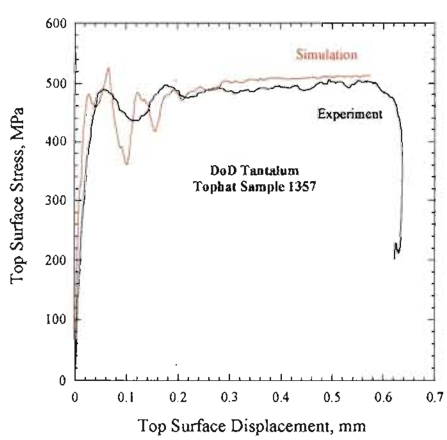

Top Hat Problem: 316L Stainless Steel

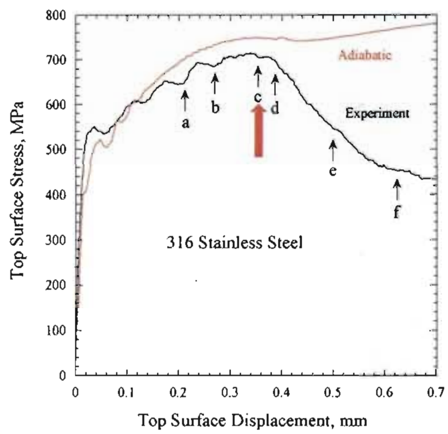

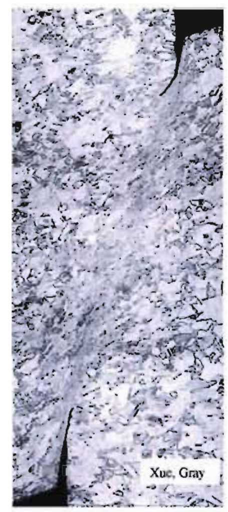

Los Alamos
NATIONAL LABORATORY

Slide 31

Operated by Los Alamos National Security, LLC for NNSA

NNSA

Top Hat Problem: 316L Stainless Steel

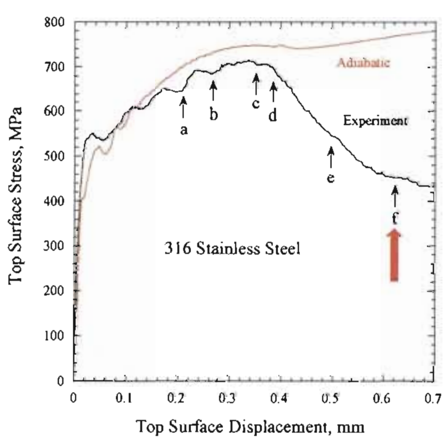

Los Alamos
NATIONAL LABORATORY

Slide 32

Operated by Los Alamos National Security, LLC for NNSA

NNSA

Sub-grid Computational Approach

Modeling Localization: Conventional vs. Embedded-zone Approach

- Localization phenomena involve a discontinuous strain field
- Conventional computational techniques
  - Can represent jumps in strain only at inter-element boundaries, not inside elements
  - Represent a localization zone as a band of elements, spanned by a single element in width, and thus yield mesh-dependent results
  - Necessitate resolving localization zones explicitly, which is prohibitively expensive, and requires a priori knowledge of the band location and orientation
- Sub-grid computational technique
  - Allows part of the localization band to be embedded inside an element, obviating the need for excessive mesh refinement
  - Allows localization band width to be specified as a material parameter, instead of being dictated by the mesh size
  - Allows band orientation to be determined based on material stability analysis
  - Allows smooth transition from uniform to localized deformation, and facilitates use of different material models inside and outside the band

Localization: Bifurcation Analysis

- Based on Hadamard (1903), Hill (1962)
- Localization zone R_L characterized by thickness *b*, unit normal *n* and strain jump direction *m*.
- Compatibility

$$[\![\dot{\varepsilon}_{ij}]\!] = \frac{1}{2} g(m_i n_j + m_j n_i)$$

- Equilibrium

$$[\![t_j]\!] = [\![n_i \dot{\sigma}_{ij}]\!] = n_i [\![\dot{\sigma}_{ij}]\!] = 0$$

- Constitutive relations

$$\dot{\sigma}_{ij} = D_{ijkl}\dot{\varepsilon}_{kl}$$

- Combined, they lead to: Find *n* and *m* such that

$$(n_i D_{ijkl} n_l) m_k = 0 \implies \det(n_i D_{ijkl} n_l) = 0$$

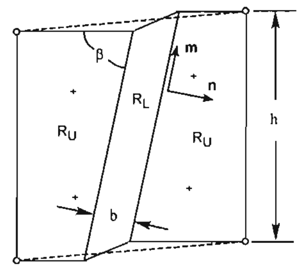

Enhanced Assumed Strain (B-bar) Method

- Based on the work of Belytschko et al (1988), Fish and Belytschko (1988)
- Conventional FEM approximation

$$u_i = N_i^A d^A, \quad \varepsilon_{ij} = B_{ij}^A d^A$$

- Strain field is continuous within elements

$$\varepsilon_{ij} = \frac{1}{2}\left(\frac{\partial u_i}{\partial x_j} + \frac{\partial u_j}{\partial x_i}\right), \quad B_{ij}^A = \frac{1}{2}\left(\frac{\partial N_i^A}{\partial x_j} + \frac{\partial N_j^A}{\partial x_i}\right)$$

- Introduce assumed strain field $\bar{\varepsilon}$ such that

$$\Delta\bar{\varepsilon}_{ij} = \bar{B}_{ij}^A \Delta d^A$$

- Constitutive relations

$$\sigma = \Sigma(\bar{\varepsilon})$$

- Internal force vector in the explicit Central Difference Method

$$M^{AB}\ddot{d}^B = (f_{ext}^A - f_{int}^A), \quad f_{int}^A = \int_\Omega \bar{B}_{ij}^A \Sigma_{ij}(\bar{\varepsilon})\, d\Omega$$

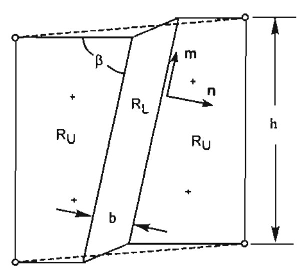

Enhanced Assumed Strain (B-bar) Method

- Weak discontinuity is characterized by
  $$T = \frac{1}{2}(m \otimes n + n \otimes m)$$
- Projection of $\Delta\varepsilon$ onto discontinuous mode
  $$(\Delta\varepsilon : T)T$$
- The assumed strain field takes the form
  $$\Delta\bar{\varepsilon}_{ij} = \Delta\varepsilon_{ij} + \alpha\,(\Delta\varepsilon_{kl}T_{kl})\,T_{ij}$$
- Recall that, by definition, $\Delta\bar{\varepsilon}_{ij} = \bar{\mathrm{B}}^{A}_{ij}\,\Delta \mathrm{d}^{A}$
- The B-bar operator has the form
  $$\bar{\mathrm{B}}^{A}_{ij} = (\delta_{ik}\delta_{jl} + \alpha\,T_{kl}T_{ij})\mathrm{B}^{A}_{kl}$$
  where $\alpha = \alpha^{L}$ in R_L, and $\alpha = -\alpha^{N}$ in R_U.
- Modified Gauss quadrature scheme
  $$\int_{\Omega^e} f(x)\,d\Omega \approx \sum_{q}^{N_q} f(x_q)\,J(\xi_q)\,W_q \;\Rightarrow\; \int_{\Omega^e} f(x)\,d\Omega \approx \sum_{q}^{N_q}\left[\frac{b}{h}f^{L}(x_q) + \left(1-\frac{b}{h}\right)f^{N}(x_q)\right]J(\xi_q)\,W_q$$

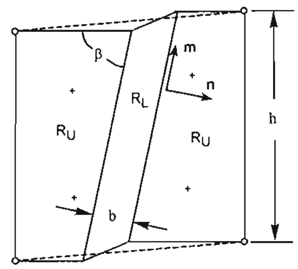

Enhanced Assumed Strain (B-bar) Method

- The unit normal vector n is known. Must determine the unit strain jump vector m, and the scalars α^{L} and α^{N}
- Equivalence between strain fields
  $$\int_{\Omega}(\bar{\mathbf{B}}^{A} - \mathbf{B}^{A})\,d\Omega = 0$$
- Definition of m as a unit vector
  $$\|m\| = 1$$
- Equilibrium at the band-matrix interface
  $$[\![t]\!] = n \cdot [\![\sigma]\!] = 0$$
- Traction continuity condition is enforced at each Gauss point, at the end of each time step, using an iterative solution scheme.

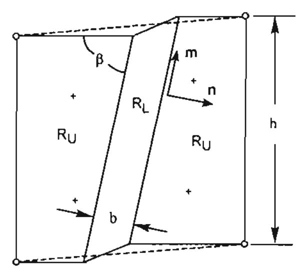

Numerical Examples

Strain Softening: A Prerequisite for Localization

- Softening gives rise to material instability
  $$\det(n_i D_{ijkl} n_l) = 0$$
- Mechanisms of material softening include
  - Thermai softening: heating due to plastic work
  - Damage (voids and/or cracks)
  - Dynamic recrystallization
- For simplicity, we choose an isotropic elastic-plastic material model, with linear isotropic hardening/softening:
  - Elastic parameters: $E = 200$ GPa, $\nu = 0.29$
  - Strength parameters:
    $\sigma_y = 300$ MPa, $\sigma_u = 310$ MPa
    $K_h = 220$ MPa, $K_s = -66$ MPa
  - Mass density, $\rho = 7850$ kg/m^3

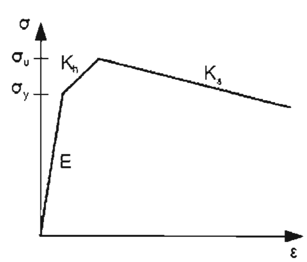

Extension of Rectangular Block

- Dimensions: $L = 0.14$ m, $w = 0.10$ m
- Upper-right quadrant modeled using three meshes to test results for mesh dependence
  - Mesh 1:
    5 ´ 7 embedded-zone elements, $b/h = 1/3$
  - Mesh 2:
    10 ´ 14 embedded-zone elements, $b/h = 2/3$
  - Mesh 3:
    15 ´ 21 conventional elements, $b/h = 1$
- Band width $b = 3.33$ mm is assumed
- Bottom-left element is weakened
- Shaded area represents localization zone detected by bifurcation analysis

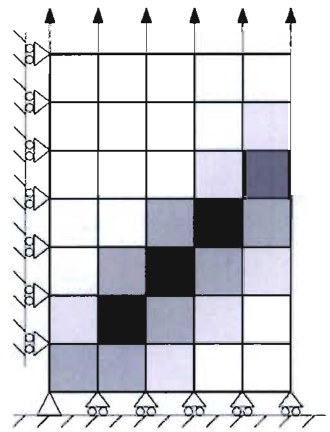

Extension of Rectangular Block

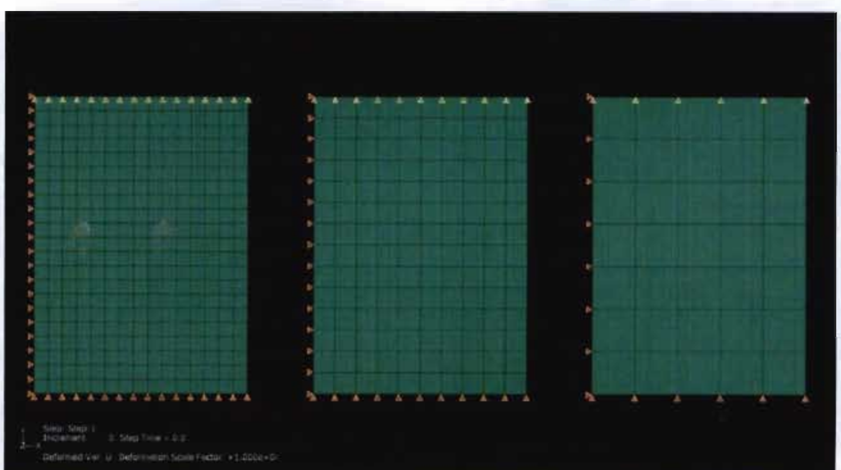

Extension of Rectangular Block

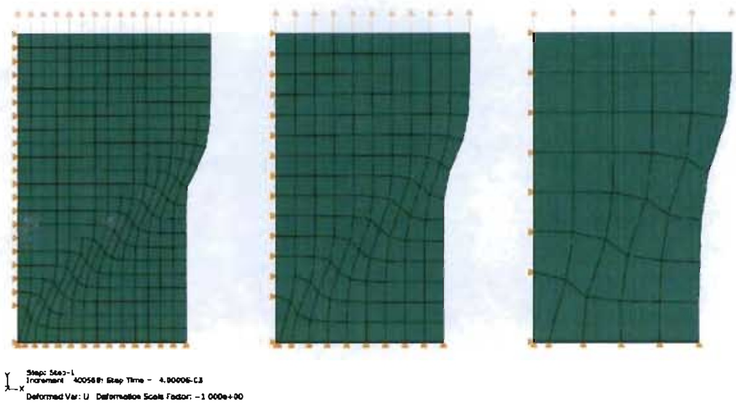

- Location and orientation of band, and its effect on overall deformation, are captured reasonably well, even by coarsest mesh.

Los Alamos
NATIONAL LABORATORY

Slide 43

Operated by Los Alamos National Security, LLC for NNSA

NNSA

Extension of Rectangular Block

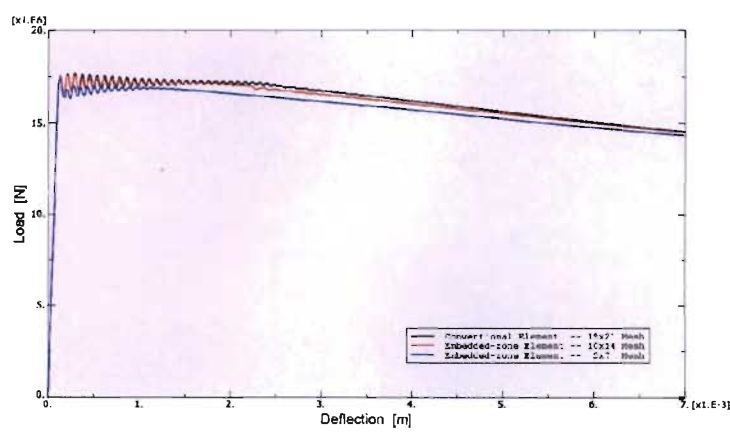

- Correct structural response is captured throughout loading process

Los Alamos
NATIONAL LABORATORY

Slide 44

Operated by Los Alamos National Security, LLC for NNSA

NNSA

Top Hat Problem: Stainless Steel

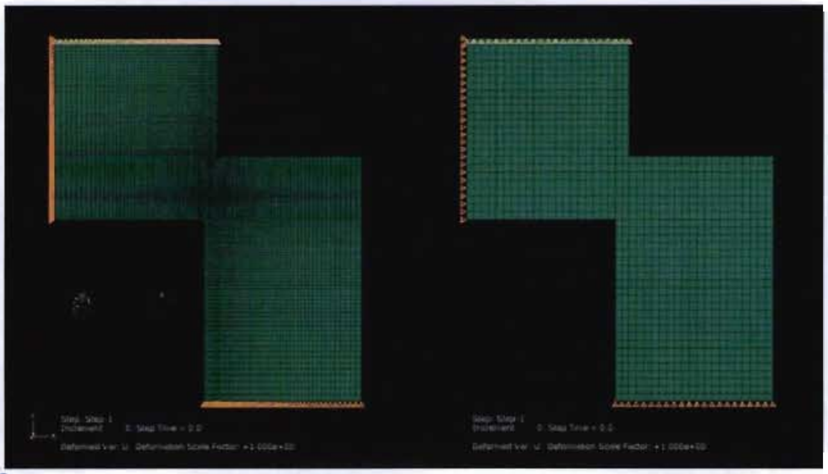

Concluding Remarks

- A sub-grid finite element formulation for modeling strain localization was presented, and its implementation within an explicit Lagrangian framework was described
- The method can treat
  - Plane-strain and axisymmetric problems
  - Small-deformation and finite-deformation problems
  - Compressible and incompressible material behavior
  - Problems involving highly-dynamic loading
- Focus of current and future work
  - Accounting properly for softening mechanisms like damage (e.g. Johnson and Addessio, 1988), thermal softening (e.g. Anand, 1985), and dynamic recrystallization

Summary & comments

- Damage and failure in polycrystalline metallic materials is strongly dependent upon microstructural details – modern lower length scale tools are necessary to assist in our learning about these complex physical processes. This can then properly motivate the development of physically based higher length scale models for use in applications.
- In general, we do not have the ability to adequately represent the topology of polycrystalline microstructures – this is especially true in 3D. Sub-granular initial state is also a concern.
- The modeling results compare OK with experimental measurements. Comments are:
  - Stress response is consistently over-predicted.
  - Texture prediction clearly shows 2D deformation gradient.
  - Shear zone strain profile is well predicted.
  - Due to tessellation limitations, triangular elements were required.

Single Crystal Work

Asaro and Rice, 1977
Asaro, 1979
Chang and Asaro, 1981

Tension

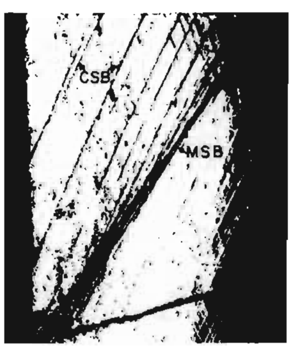

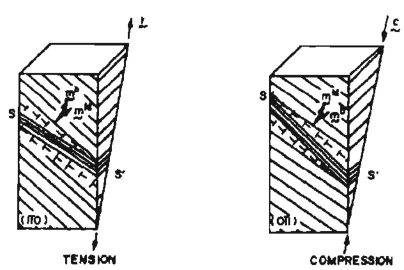

- Single crystals of Al-2.8Cu with θ' and θ precipitate particles
- Course slip bands were aligned with the active slip systems
- Macroscopic shear bands were preceded by the formation of coarse slip bands but were not aligned with active slip systems.

Los Alamos
NATIONAL LABORATORY
Operated by Los Alamos National Security, LLC for NNSA
NNSA

Polycrystal Work

Bronkhorst et al. (1992)
Anand & Kalidindi (1994)

Plane Strain Compression

OFHC Cu

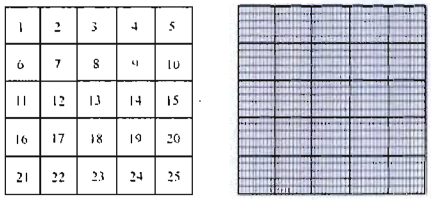

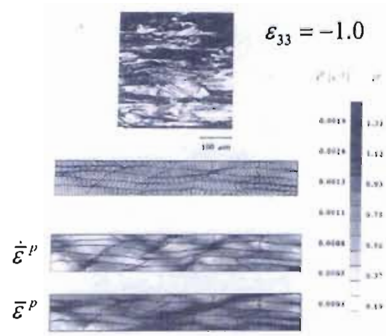

- Each of the 25 crystals was divided into 50 equal-sized elements.
- Localization into zones oriented 30-40° from horizontal.
- Shear banding is a natural part of inhomogeneous large deformation process and is closely linked with evolution of crystallographic texture.

Single Crystal Work

Wang, Beyerlein, LeSar (2006, 2007)

Talk on Tuesday 8:00

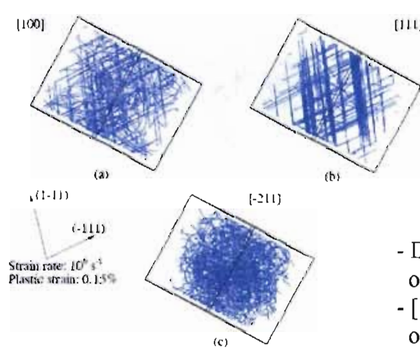

- Dislocation dynamics on Cu at rates of deformation $10^4 - 10^6$ s^{-1}.
- [100], [111], [-211] tensile loading orientations.
- Inhomogeneous dislocation accumulation leads to "directional" microstructure.
- Slip bands developing on the more active slip systems, particularly for [111] orientation.

Single/Polycrystal Work

Cheong & Busso (2006)

Tension

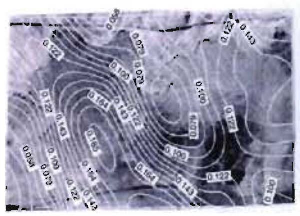

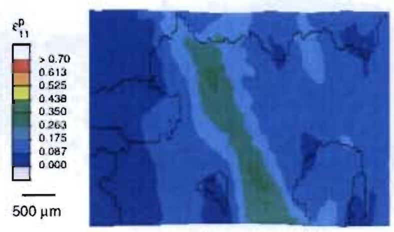

(b) Case 2 (max $\varepsilon^p_{11} = 0.36$)

- Modeled the tension response of large grain "sheet" sample.
- Able to represent the qualitative profile of localized deformation.
- Required inclusion of misorientation distribution within the large crystals to represent the magnitude correctly.

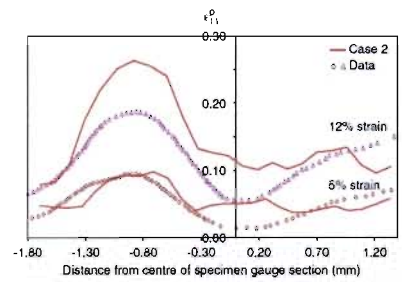

Polycrystal Work

Becker (1992)

Aluminum

Bending

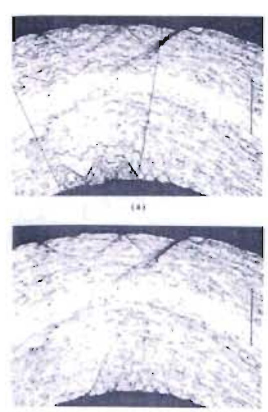

- Taylor-type model applied to each integration point using 8 grains chosen at random from a distribution of 800 grains.
- Resistance to shear band growth by grains which are not favorably oriented.
- Overall localization planes are formed at reasonable strain levels and at appropriate orientations.

Tophat Experiments

Results from tophat experiments performed at 25 C

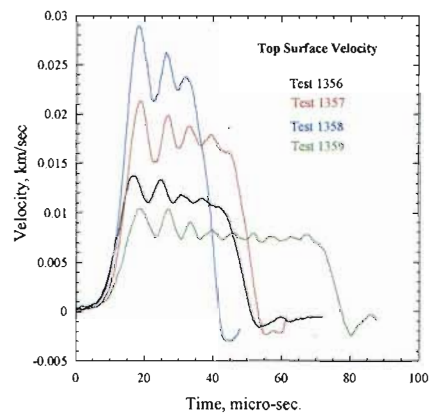

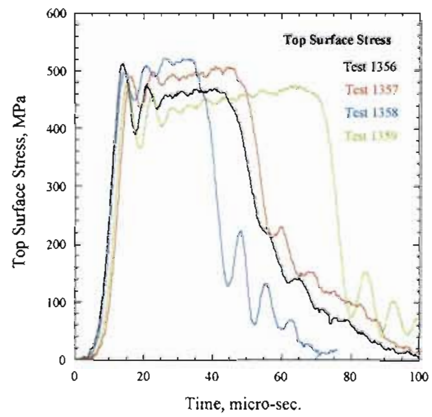

Los Alamos NATIONAL LABORATORY

Operated by Los Alamos National Security, LLC for NNSA

NNSA

Localization - Ta

- Dynamic response of the SHPB system is not represented
- Piecewise linear velocity profile applied uniformly to the top surface
- Top surface stress response is weighted average of top row of elements

Velocity profile at -100 °C

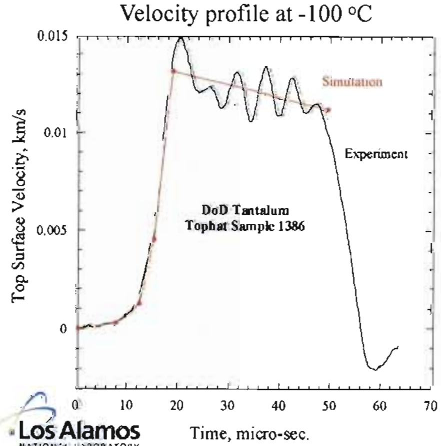

Predicted response at -100 °C

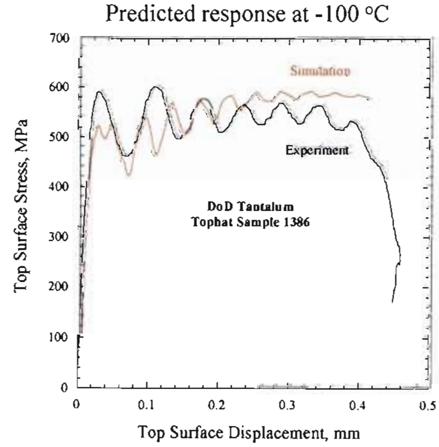

Los Alamos NATIONAL LABORATORY

Operated by Los Alamos National Security, LLC for NNSA

NNSA

Localization

- FE code EPIC - explicit
- Axisymmetric and adiabatic
- 46,000 triangular elements
- 2000 shear section elements
- Contact friction surfaces in two corners
- Velocity profile applied to top surface
- Rigid and frictionless base
- Stress response at top surface compared to experiments

Low density mesh shown

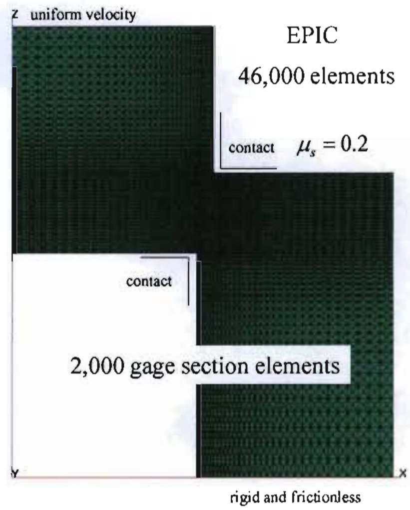

Continuum Model

Addessio and Johnson, 1993; Maudlin et al., 1999
Mason, 1999, 2004

Stress

$$\mathbf{T} = \mathbf{M}\tilde{\mathbf{T}} \qquad \underline{\mathbf{M}} = (1-\phi)\underline{\mathbf{I}}$$

$$\dot{\mathbf{T}} = \underline{\mathbf{M}}\underline{\mathbf{L}}^{\sim\prime}\left(\mathbf{D}' - \mathbf{D}^{p\prime}\right) - \underline{\mathbf{M}}\left(-\frac{\partial\tilde{P}}{\partial\beta}\mathrm{tr}\mathbf{D}^e + \frac{\tilde{\rho}}{\rho}\Gamma\mathbf{T}\cdot\mathbf{D}^p\right)\underline{\mathbf{I}} + \dot{\underline{\mathbf{M}}}\underline{\mathbf{M}}^{-1}\mathbf{T}$$

Strain Rate

$$\mathbf{D} = \mathbf{D}^e + \mathbf{D}^p = \mathbf{D}^e + \mathbf{D}^d + \mathbf{D}^{p\prime}$$

Plastic Flow Rate

$$\mathbf{D}^p = \frac{1}{\tau_r}\left(\mathbf{T} - \mathbf{T}^{proj}\right)$$

$\tau_r = 70$ Pa·s
$q_1 = 1.5$
$q_2 = 0.625$
$q_3 = 2.25$

$$\tau - \sigma_f\left(\dot{\varepsilon},\theta\right)^2\left[1 + q_3\phi^2 - 2q_1\phi\cosh\delta\right] = 0$$

$$\tau = \frac{1}{2}\mathbf{T}'\cdot\underline{\alpha}\cdot\mathbf{T}' \qquad \delta = -\frac{3q_2\tilde{P}}{2\sigma_s} \qquad \tilde{P} = -\tfrac{1}{3}\mathrm{tr}\tilde{\mathbf{T}}$$

Damage Rate $\quad \mathrm{tr}\mathbf{D}^p > 0$

$$\mathbf{D}^d = \frac{\dot{\phi}}{3(1-\phi)}\underline{\mathbf{I}} \qquad \dot{\phi} = (1-\phi)\mathrm{tr}\mathbf{D}^p$$

$\phi_0 = 0.0003$

Equation of State

$$\tilde{P} = \left(K_1\tilde{\beta} + K_2\tilde{\beta}^2 + K_3\tilde{\beta}^3\right)\left(1 - \Gamma\tilde{\beta}/2\right) + \Gamma\tilde{E}_s\left(1 + \tilde{\beta}\right)$$

$$\tilde{\beta} = \frac{\tilde{\rho}}{\tilde{\rho}_0} - 1$$

$$\rho = (1-\phi)\tilde{\rho}$$

$K_1 = 196.8$ GPa	$\Gamma = 1.60$
$K_2 = 259.8$ GPa	$\rho_0 = 16{,}640$ kg/m^3
$K_3 = 256.6$ GPa	

Plastic Work

$$\dot{\theta} = \frac{\eta}{\rho C_p}E_s$$

$\eta = 0.95$
$C_p = 54.4$ J/kg·K

Localization - Ta

- Predicted responses for sample 1356 and 1357 experiments performed at 25 °C

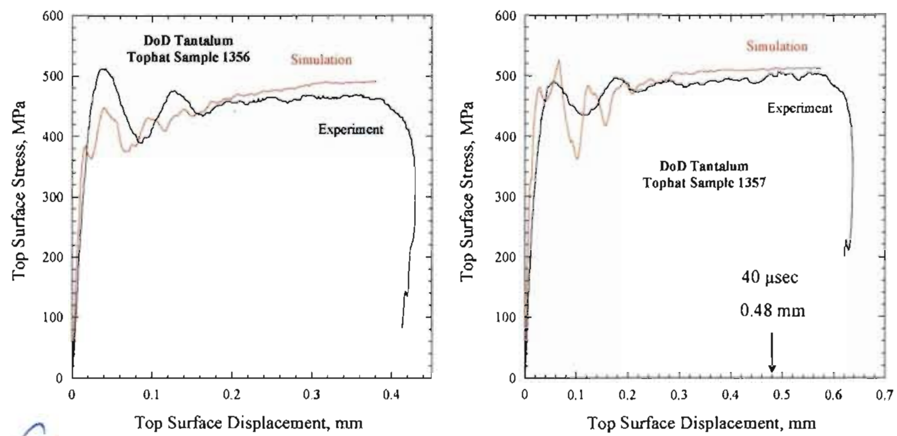

Los Alamos NATIONAL LABORATORY

Operated by Los Alamos National Security, LLC for NNSA

NNSA

Continuum Model – Sample 1357

Time = 40 micro-sec.

- Contact friction significant in top corner
- Damage plays no role
- Shear band does not form

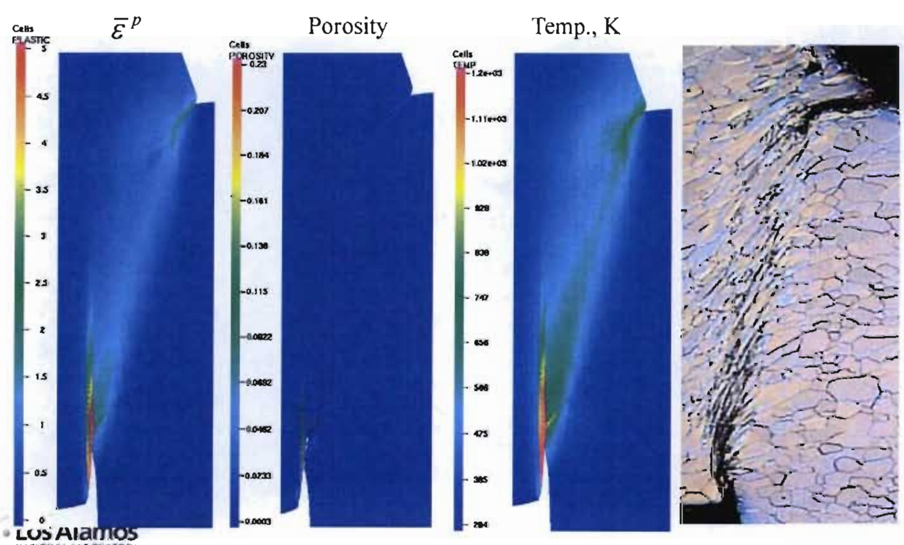

Los Alamos NATIONAL LABORATORY

Operated by Los Alamos National Security, LLC for NNSA

NNSA

Shear Band – 316 SS

Displacement (a)

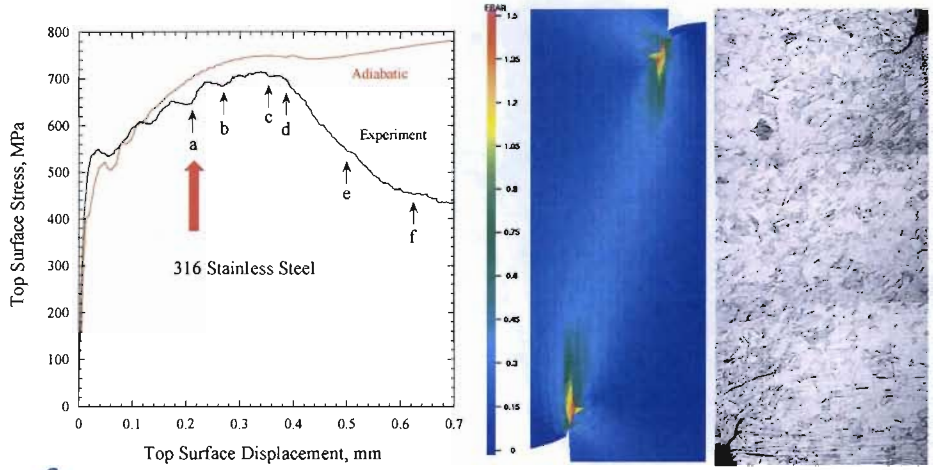

Shear Band – 316 SS

Displacement (b)

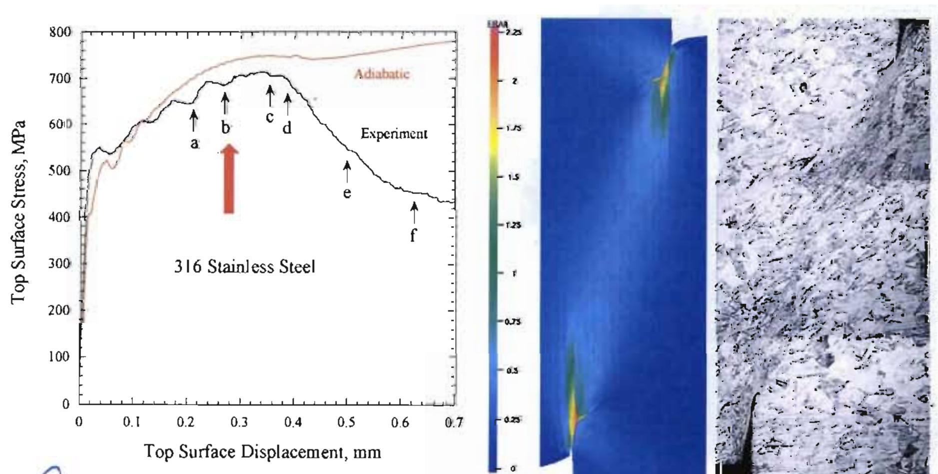

Shear Band – 316 SS

Displacement (c)

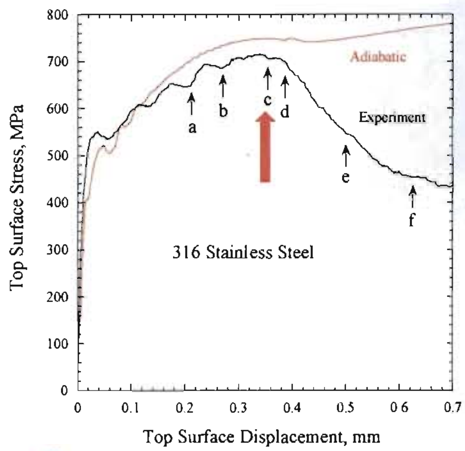

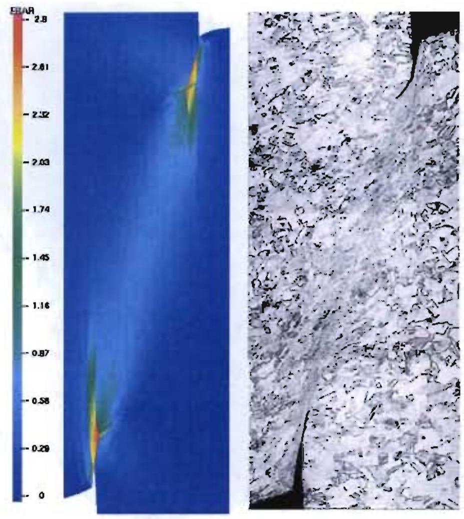

Los Alamos NATIONAL LABORATORY

Operated by Los Alamos National Security, LLC for NNSA

Shear Band – 316SS

Displacement (d)

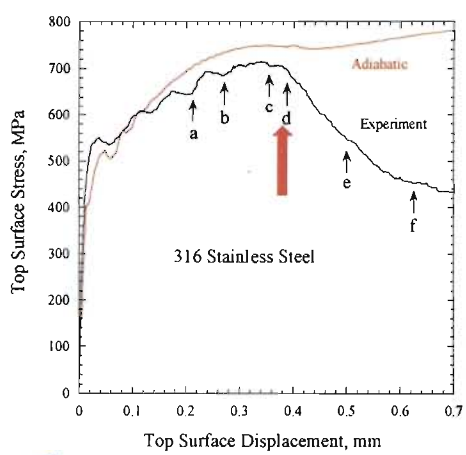

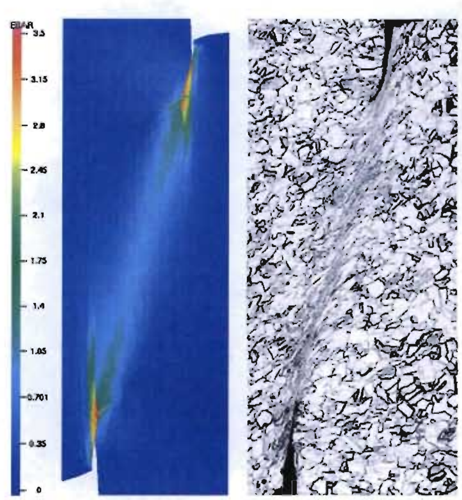

Los Alamos NATIONAL LABORATORY

Operated by Los Alamos National Security, LLC for NNSA

Shear Band – 316SS

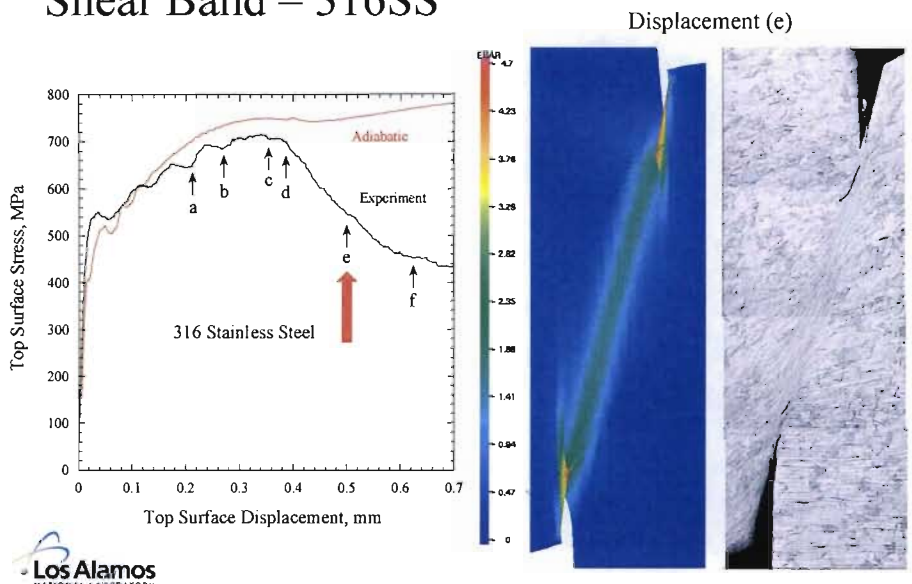

Los Alamos NATIONAL LABORATORY

Operated by Los Alamos National Security, LLC for NNSA

NNSA

Shear Band – 316 SS

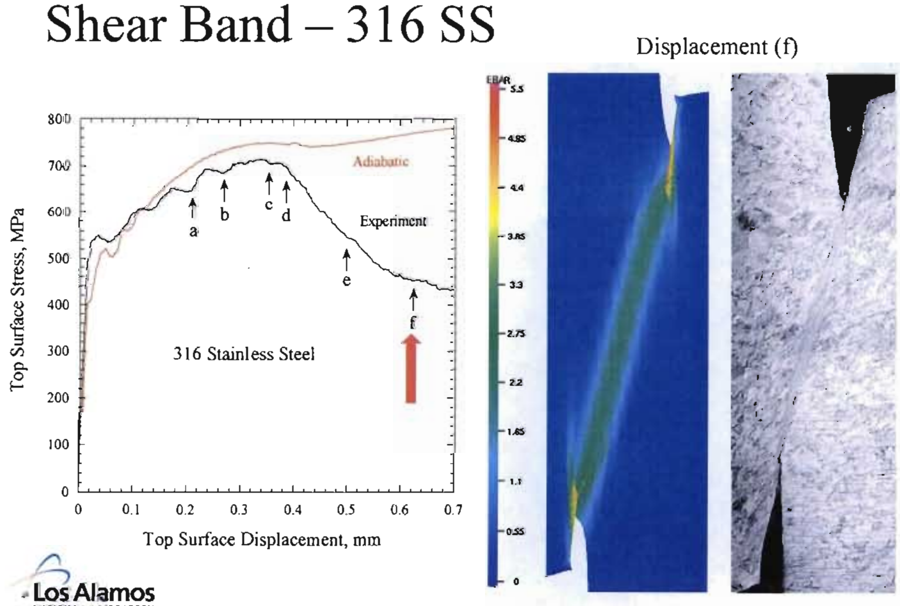

Los Alamos NATIONAL LABORATORY

Operated by Los Alamos National Security, LLC for NNSA

NNSA

Localization

- Shear and normal stress defined relative to shear zone line
- Stress in shear zone is quite uniform
- Shear zone line angle changes from 77.2° to 75.8°

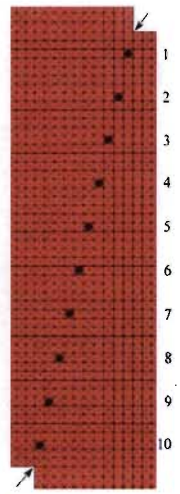

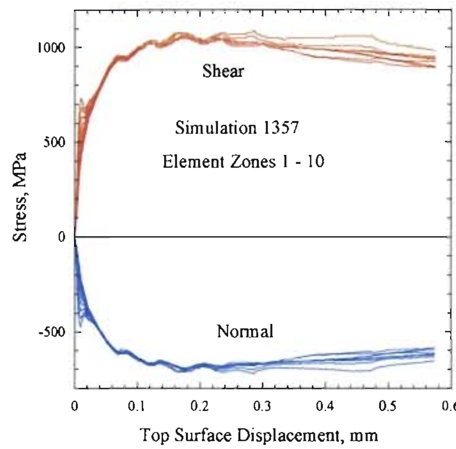

Los Alamos NATIONAL LABORATORY
Operated by Los Alamos National Security, LLC for NNSA

NNSA

Localization

- Shear zone was bisected to form separated "hat" and "brim" pieces – frictionless contact
- There is a resistance to deformation due to the expansion of the outer ring.

Two-piece, frictionless model

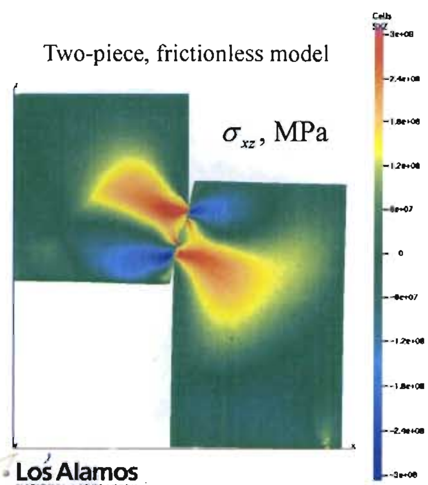

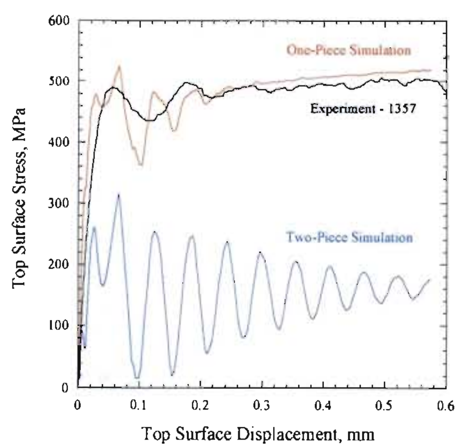

Los Alamos NATIONAL LABORATORY
Operated by Los Alamos National Security, LLC for NNSA

NNSA

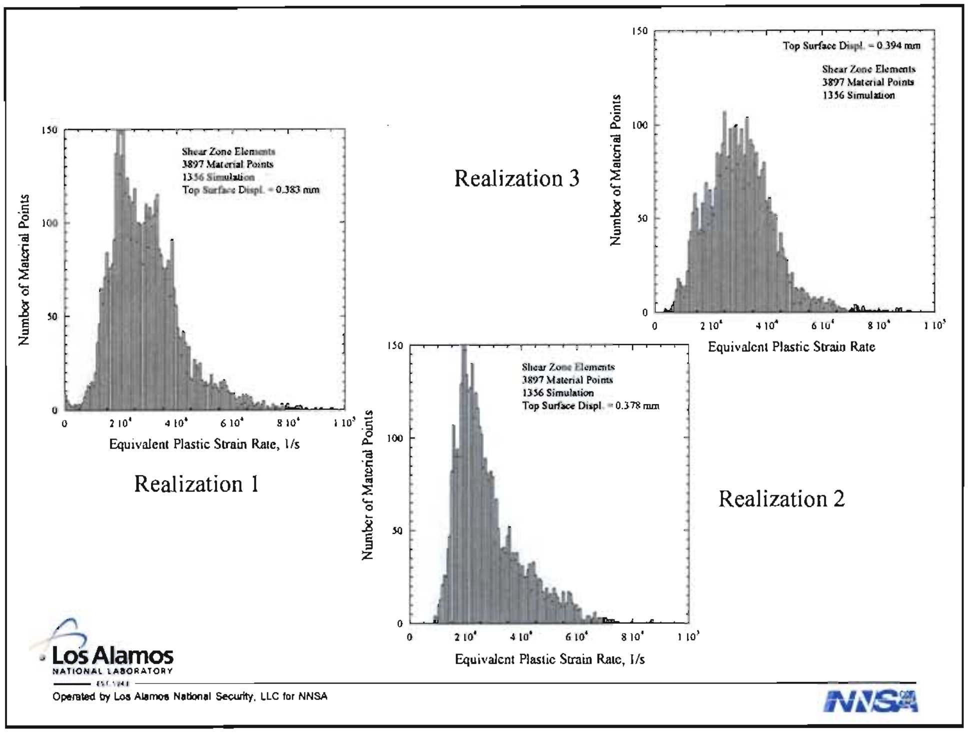
Realization 1
Realization 2
Realization 3
Shear Zone Elements
3897 Material Points
1356 Simulation
Top Surface Displ. = 0.383 mm
Top Surface Displ. = 0.378 mm
Top Surface Displ. = 0.394 mm
Number of Material Points
Equivalent Plastic Strain Rate, 1/s
Equivalent Plastic Strain Rate
Los Alamos
NATIONAL LABORATORY
Operated by Los Alamos National Security, LLC for NNSA
NNSA

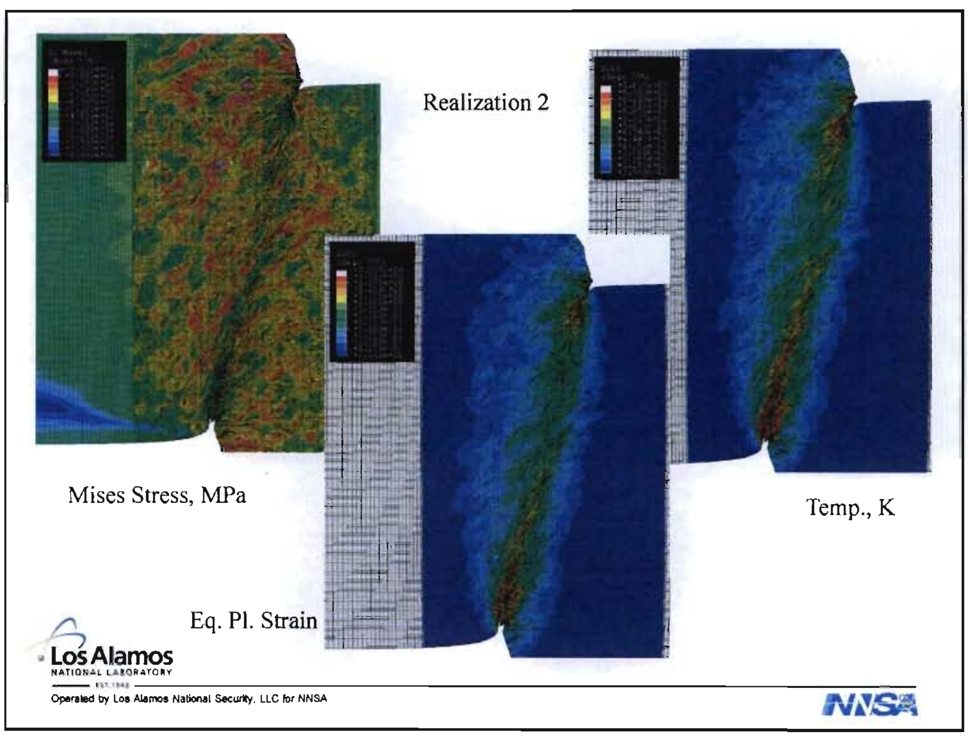
Realization 2
Mises Stress, MPa
Eq. Pl. Strain
Temp., K
Los Alamos
NATIONAL LABORATORY
Operated by Los Alamos National Security, LLC for NNSA
NNSA

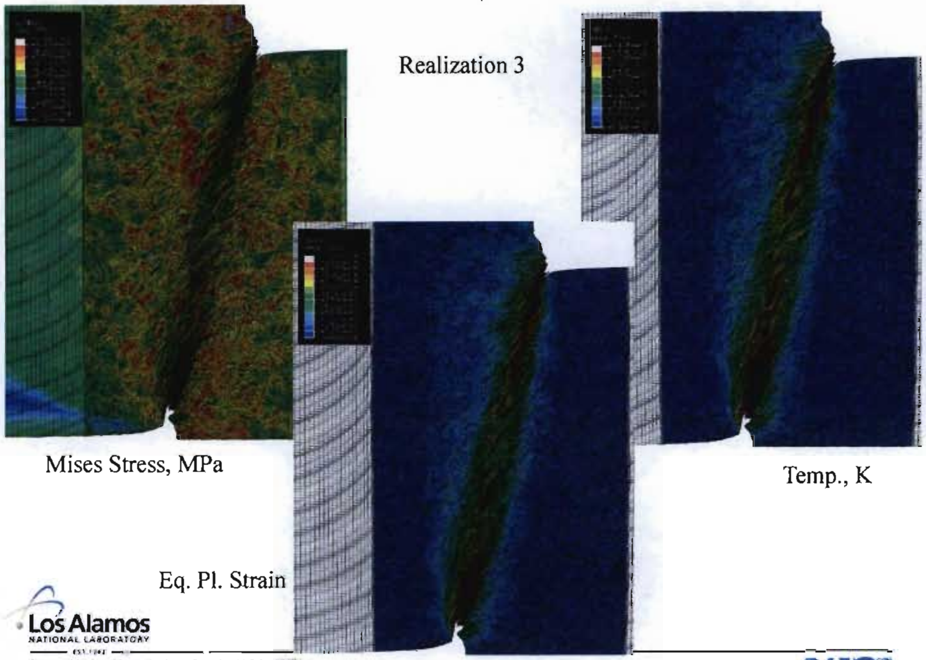

Localization - Ta

Continuum | Experimental | Realization 2 Polycrystal

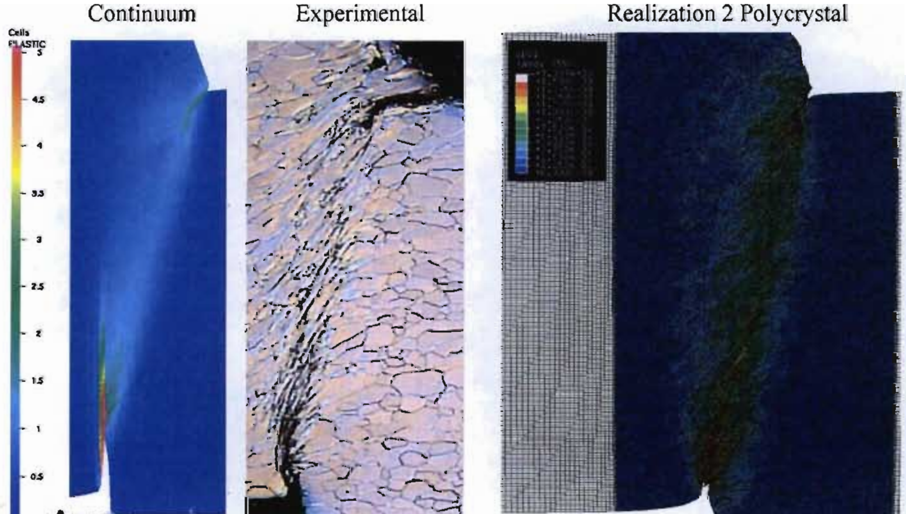

Localization - Ta

Continuum

Experimental

Realization 3 Polycrystal

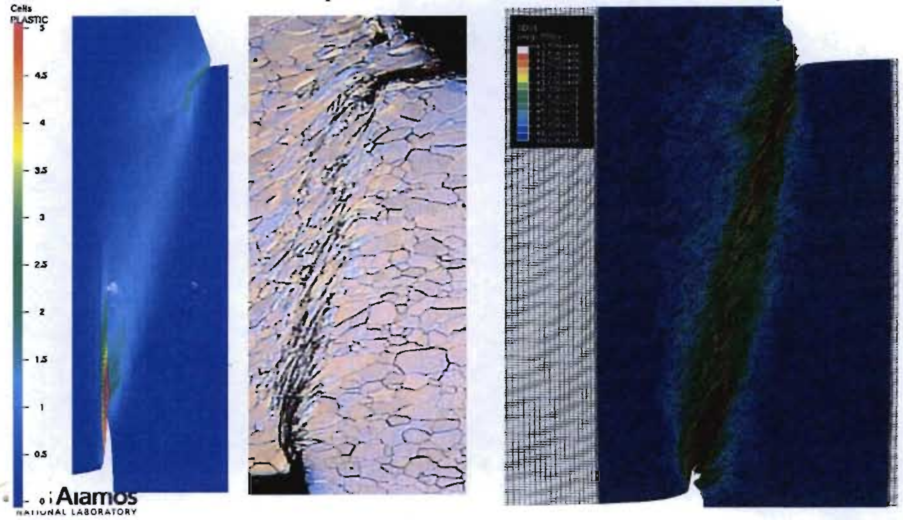

Los Alamos
NATIONAL LABORATORY
EST. 1943
Operated by Los Alamos National Security, LLC for NNSA

NNSA

Localization - Ta

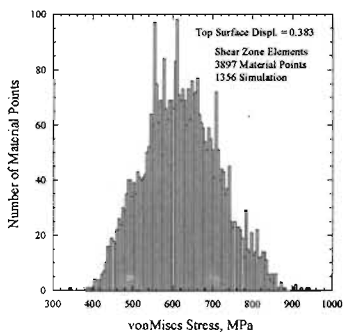

Realization 1

Realization 3

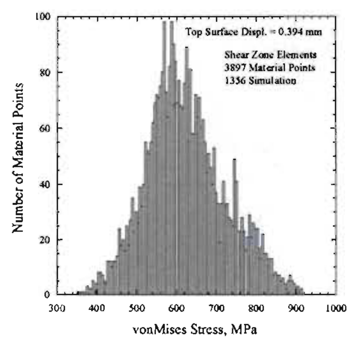

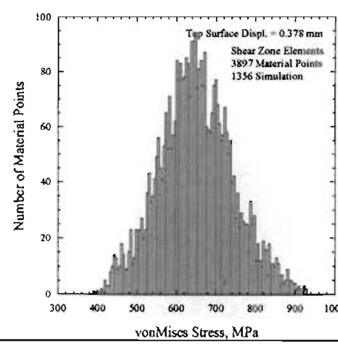

Realization 2

Los Alamos
NATIONAL LABORATORY
EST. 1943
Operated by Los Alamos National Security, LLC for NNSA

NNSA

[redacted]

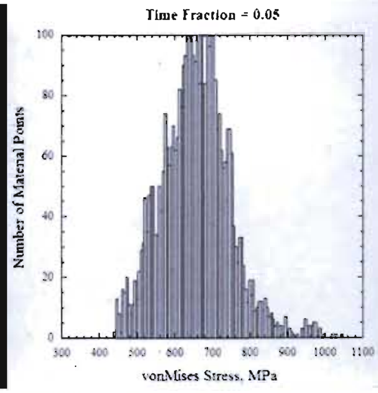

[redacted]

Realization 1

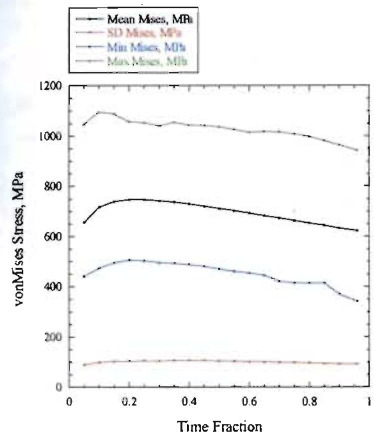

Los Alamos NATIONAL LABORATORY EST. 1943

Operated by Los Alamos National Security, LLC for NNSA

NNSA

Localization - Ta

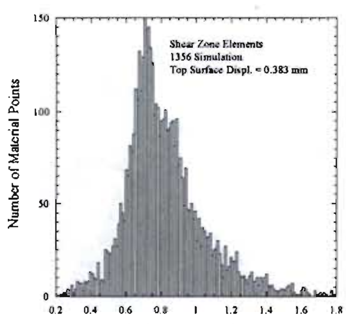

Realization 1

Realization 3

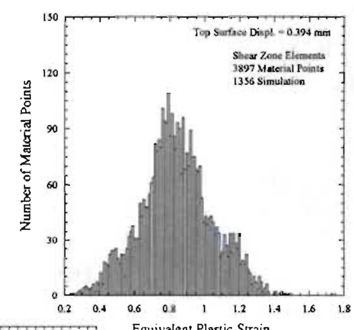

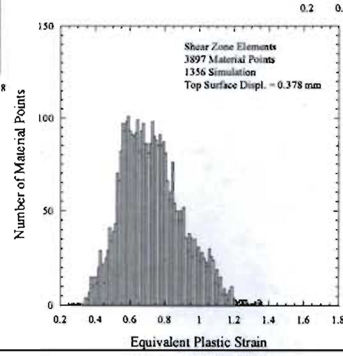

Realization 2

Los Alamos NATIONAL LABORATORY EST. 1943

Operated by Los Alamos National Security, LLC for NNSA

NNSA

Localization - Ta

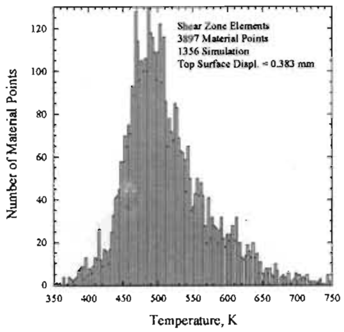

Realization 1

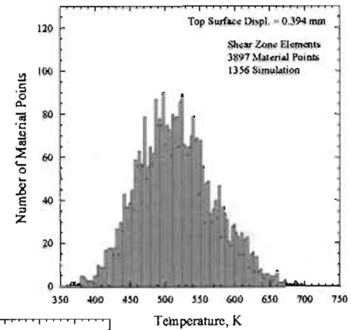

Realization 3

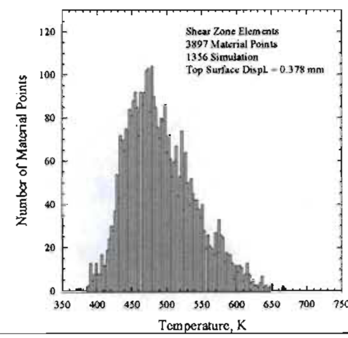

Realization 2

Los Alamos
NATIONAL LABORATORY
EST. 1943

Operated by Los Alamos National Security, LLC for NNSA

NNSA

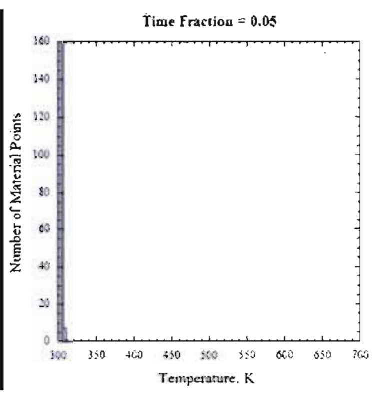

Realization 1

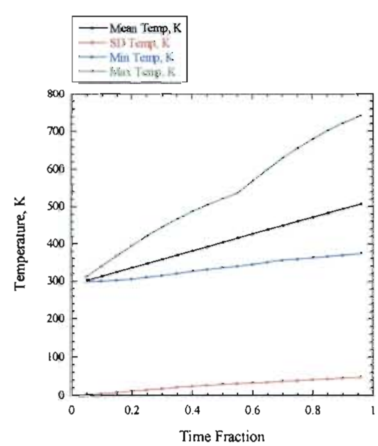

Los Alamos
NATIONAL LABORATORY
EST. 1943

Operated by Los Alamos National Security, LLC for NNSA

NNSA

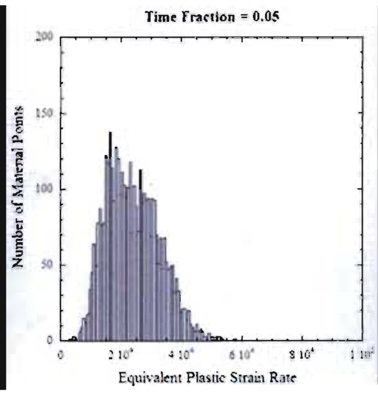

Realization 1

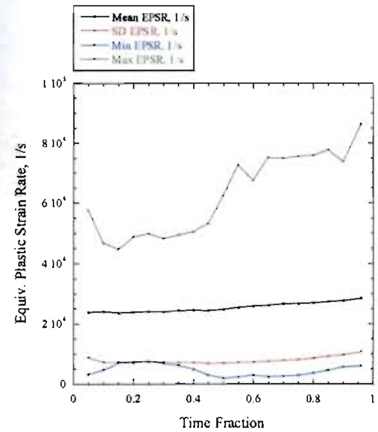

Extraction of material point information – 3 realizations

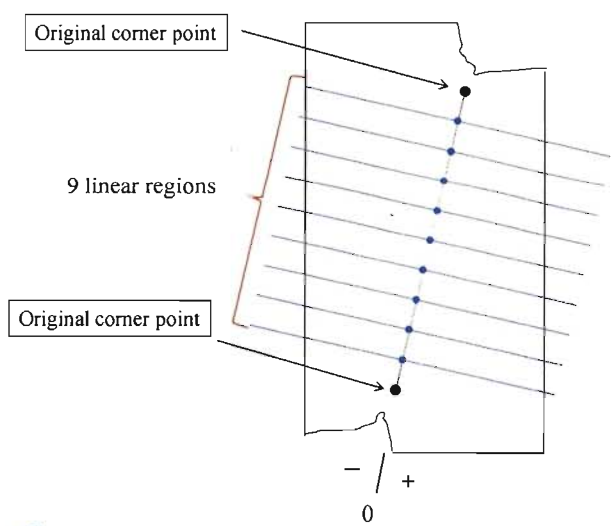

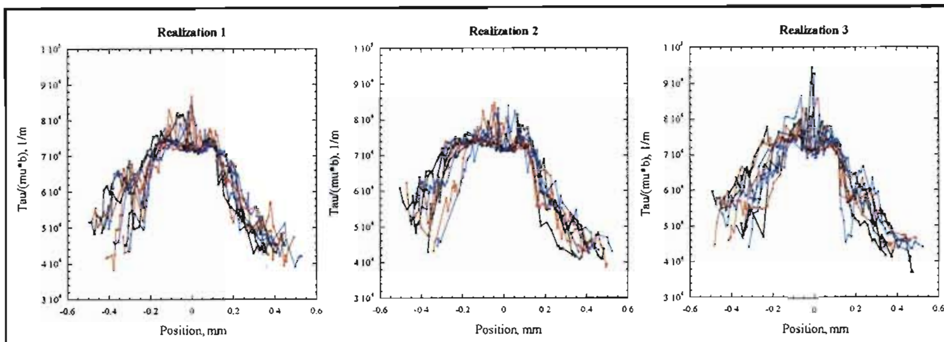

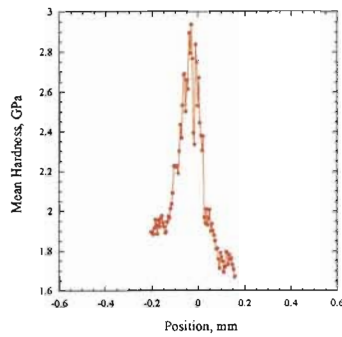

More examination of information is required

Length distribution is over-predicted but relative magnitude is first order accurate

Single measurement distribution

Extraction of material point information – 3 realizations

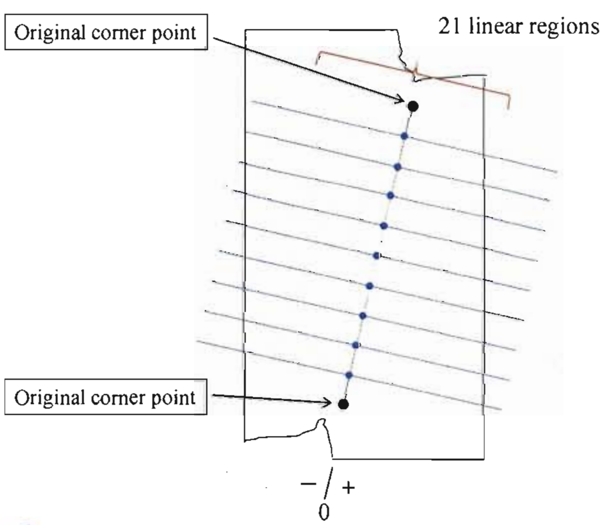

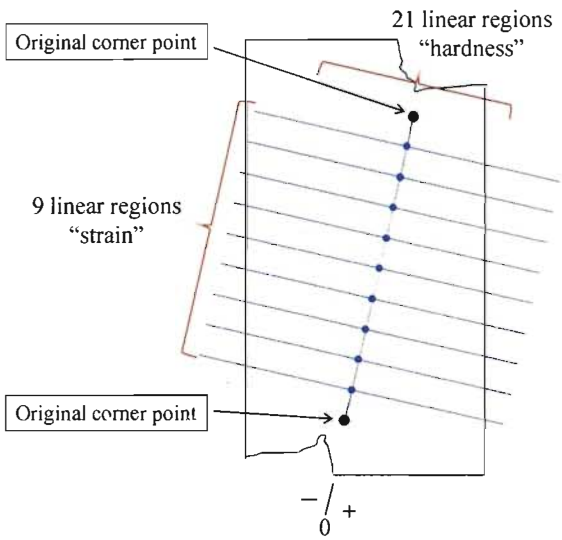

Extraction of material point information – 3 realizations